Supporting Information for

Ferrous Carbonyl Dithiolates as Precursors to FeFe-, FeCo-, and FeMn-Dithiolates

Maria E. Carroll, Jinzhu Chen, Danielle E. Gray, James C. Lansing, Thomas B. Rauchfuss,*
David Schilter, Phillip I. Volkers, and Scott R. Wilson

Page Contents

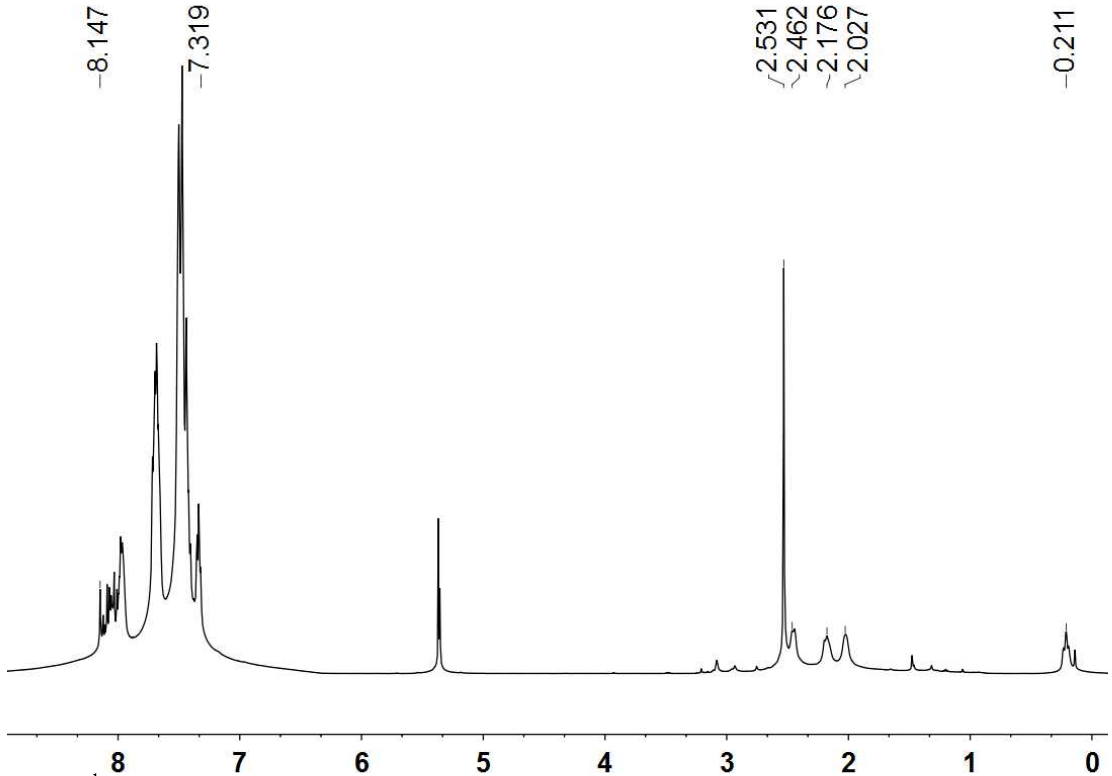

Figure S1. ^{1}H NMR spectrum (500 MHz) of $Fe(edt)(CO)_2(dppv)$ (**1a**) in CD_2Cl_2 solution.

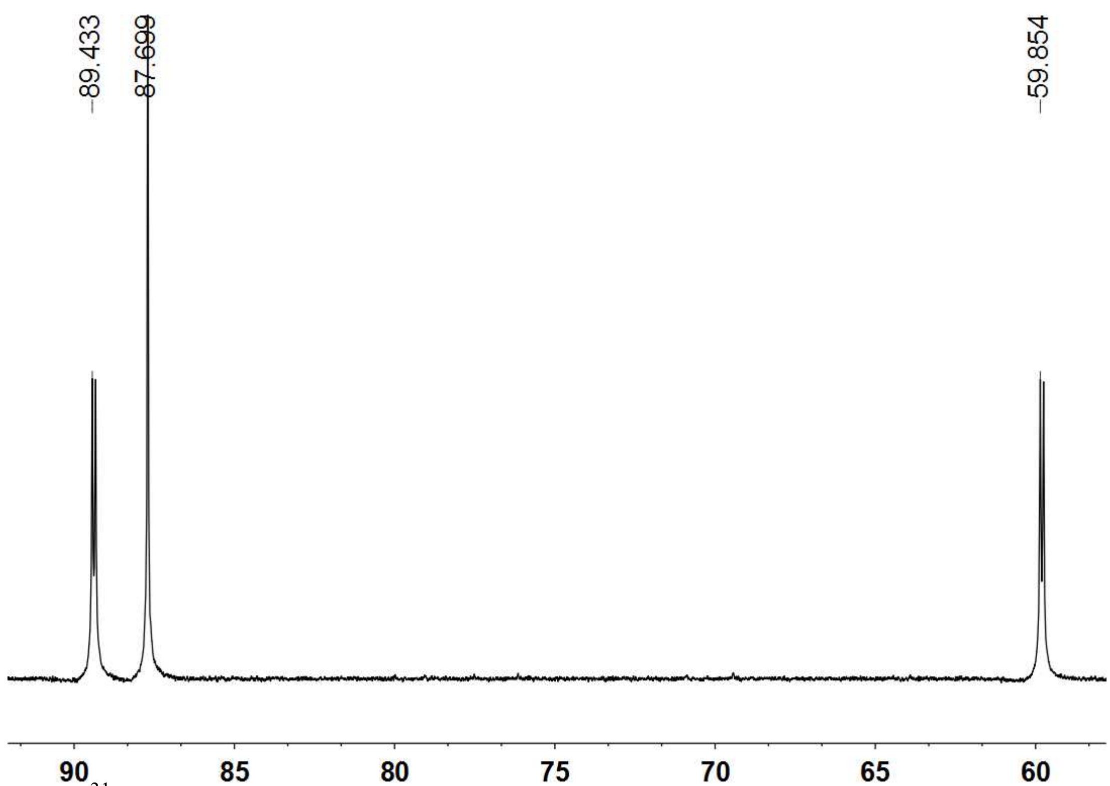

Figure S2. ^{31}P NMR spectrum (202 MHz) of $Fe(edt)(CO)_2(dppv)$ (**1a**) in CD_2Cl_2 solution.

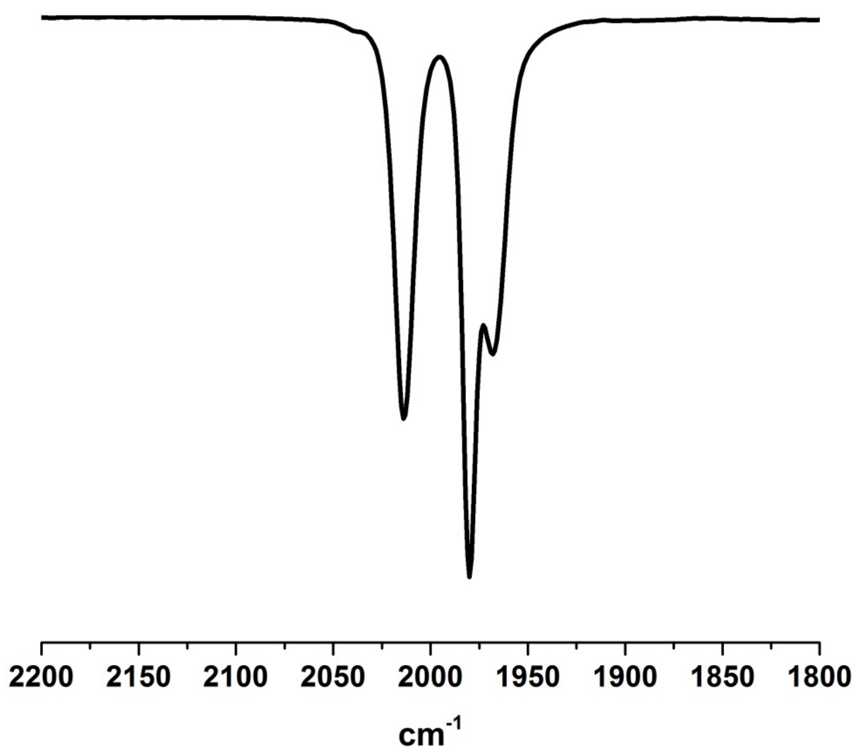

Figure S3. IR spectrum of Fe(edt)$(CO)_2$(dppv) (**1a**) in THF solution.

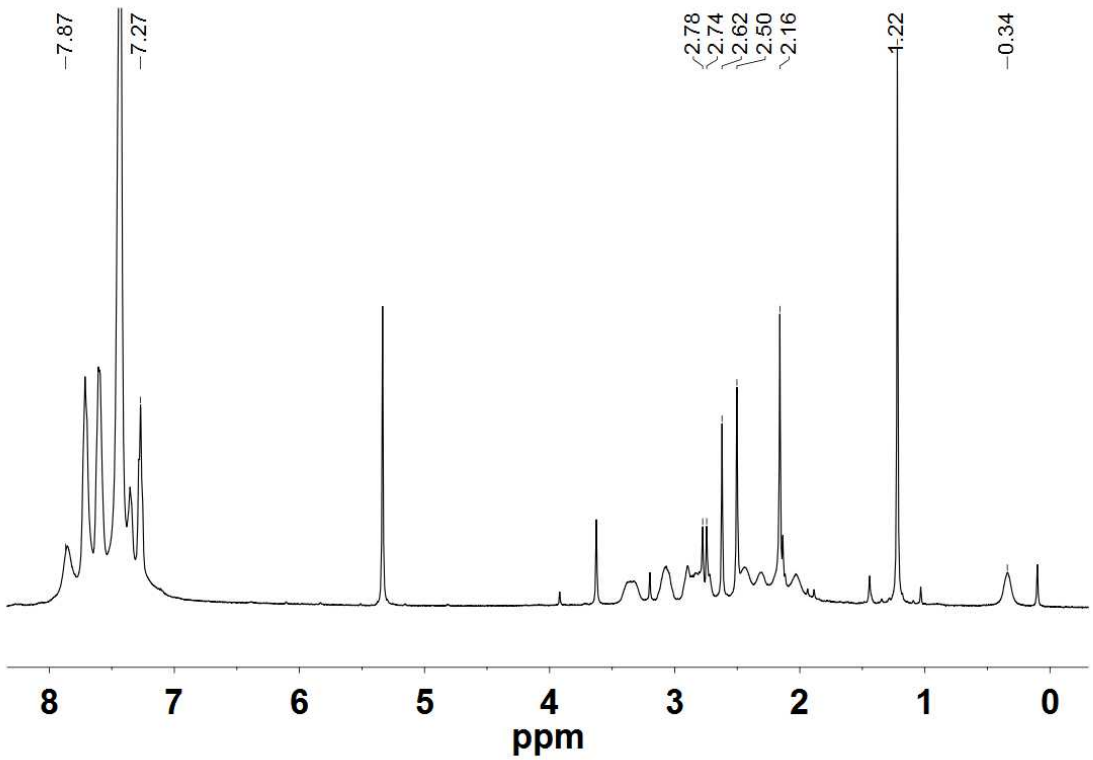

Figure S4. ^{1}H NMR spectrum (500 MHz) of Fe(edt)(CO)$_2$(dppe) (**1b**) in CD_2Cl_2 solution.

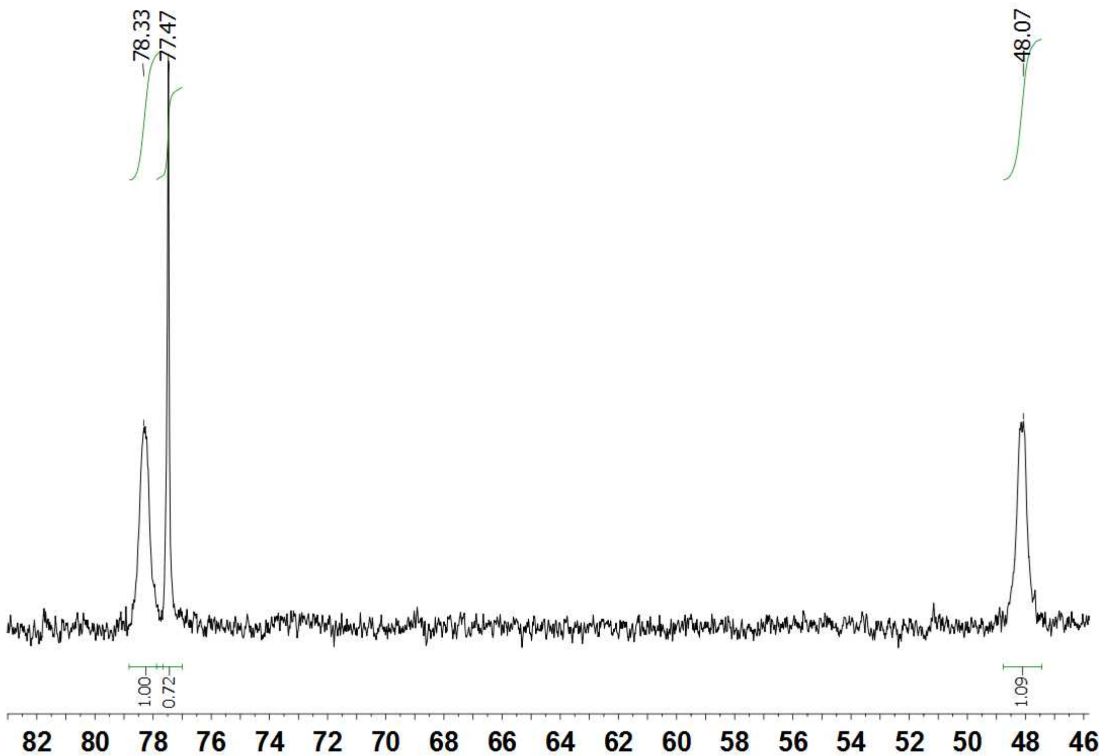

Figure S5. ^{31}P NMR spectrum (202 MHz) of Fe(edt)$(CO)_2$(dppe) (**1b**) in CD_2Cl_2 solution.

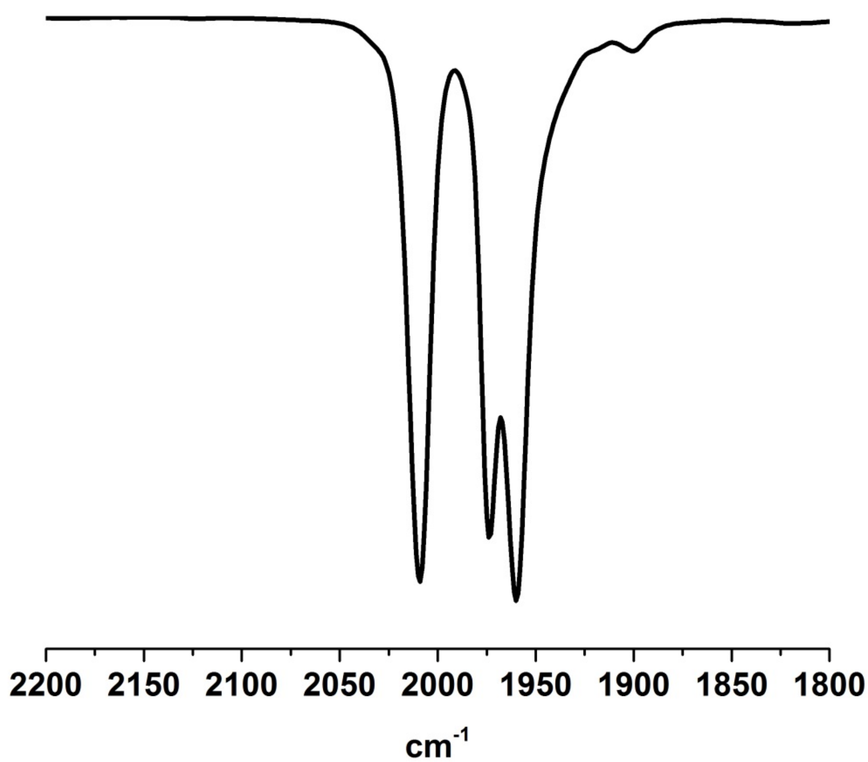

Figure S6. IR spectrum of Fe(edt)$(CO)_2$(dppe) (**1b**) in THF solution.

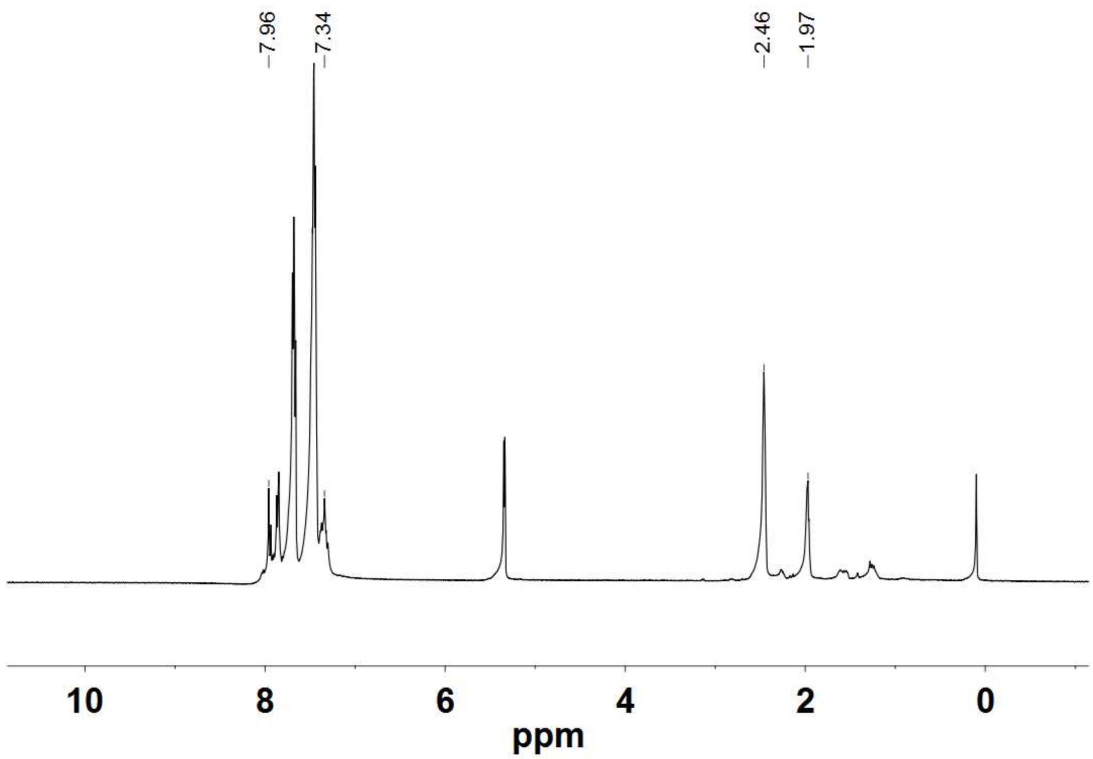

Figure S7. [1]H NMR spectrum (500 MHz) of Fe(pdt)$(CO)_2$(dppv) (**1c**) in CD_2Cl_2 solution.

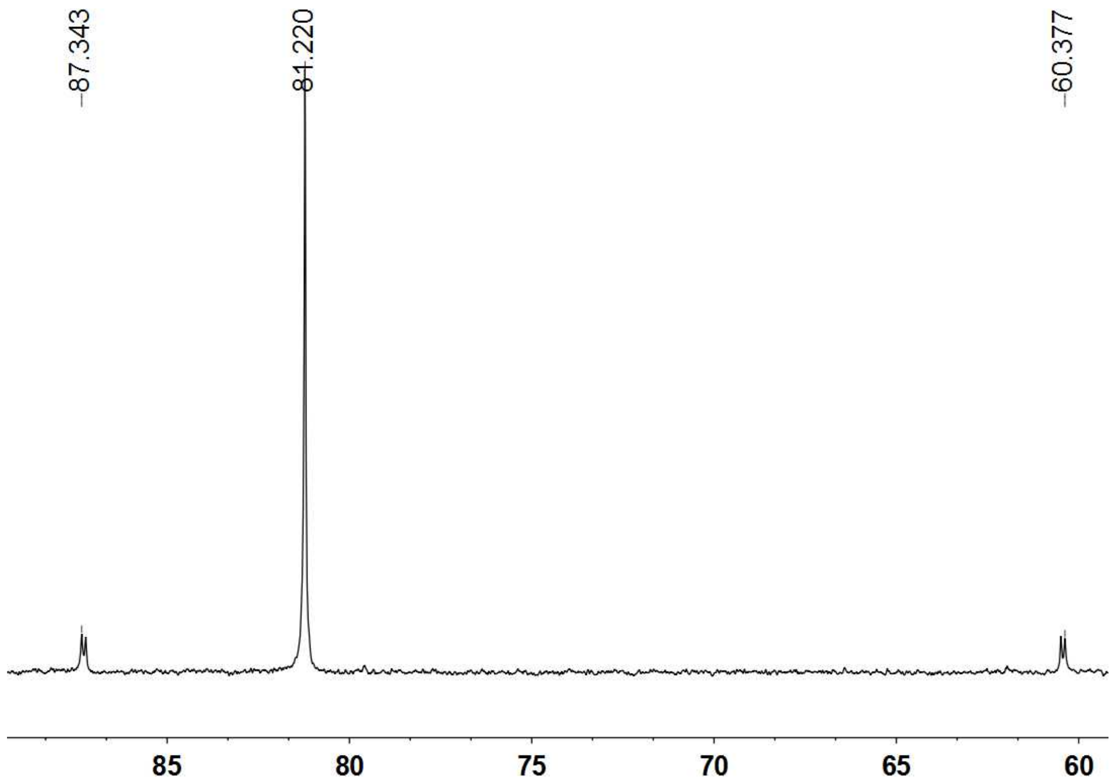

Figure S8. ^{31}P NMR spectrum (202 MHz) of Fe(pdt)(CO)$_2$(dppv) (**1c**) in CD_2Cl_2 solution.

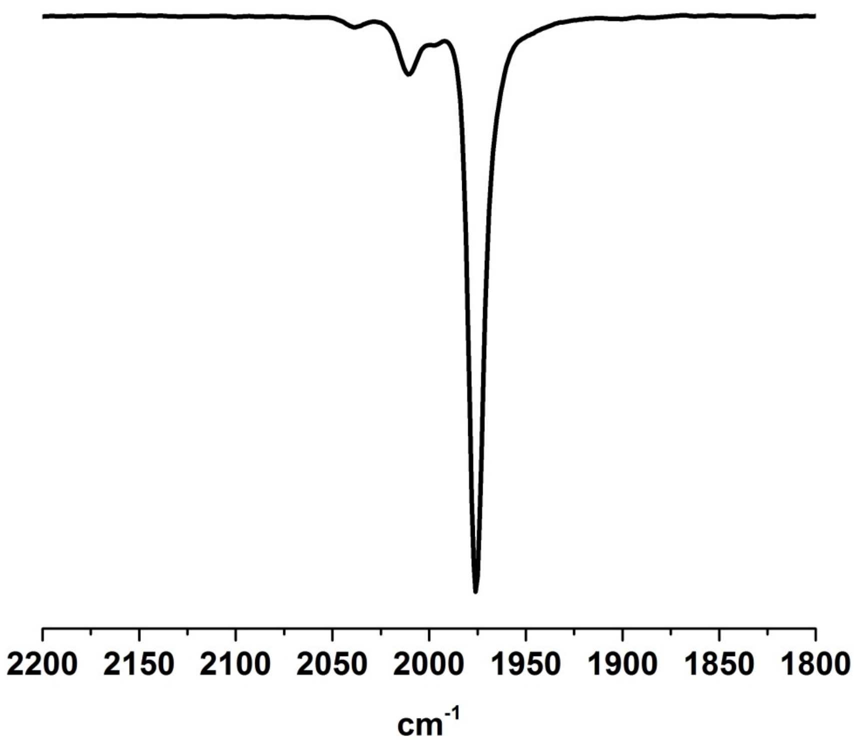

Figure S9. IR spectrum of $Fe(pdt)(CO)_2(dppv)$ (**1c**) in THF solution.

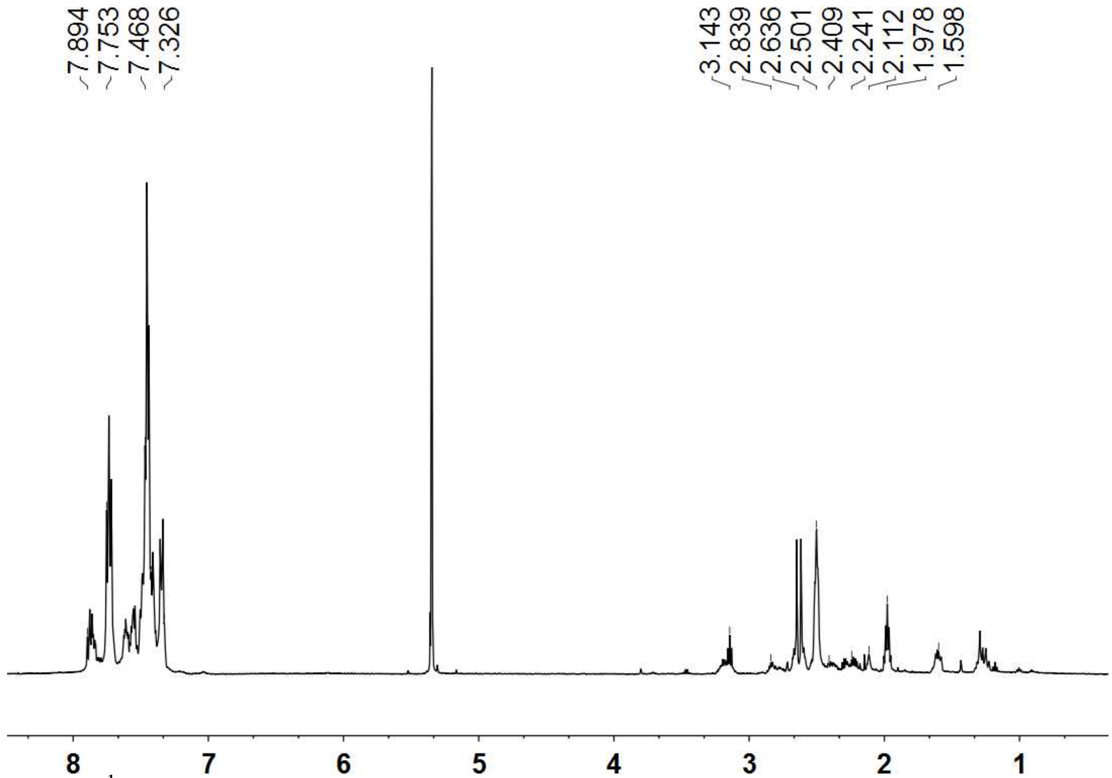

Figure S10. [1]H NMR spectrum (500 MHz) of Fe(pdt)$(CO)_2$(dppe) (**1d**) in CD_2Cl_2 solution.

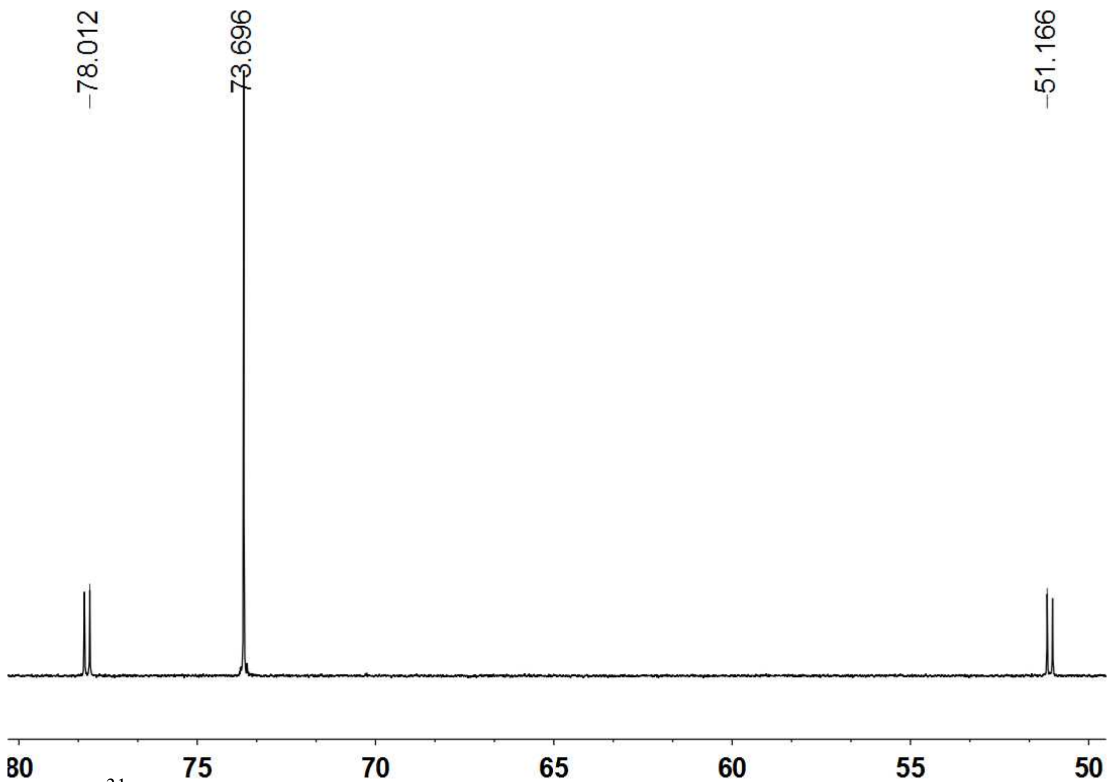

Figure S11. ^{31}P NMR spectrum (202 MHz) of Fe(pdt)$(CO)_2$(dppe) (**1d**) in CD_2Cl_2 solution.

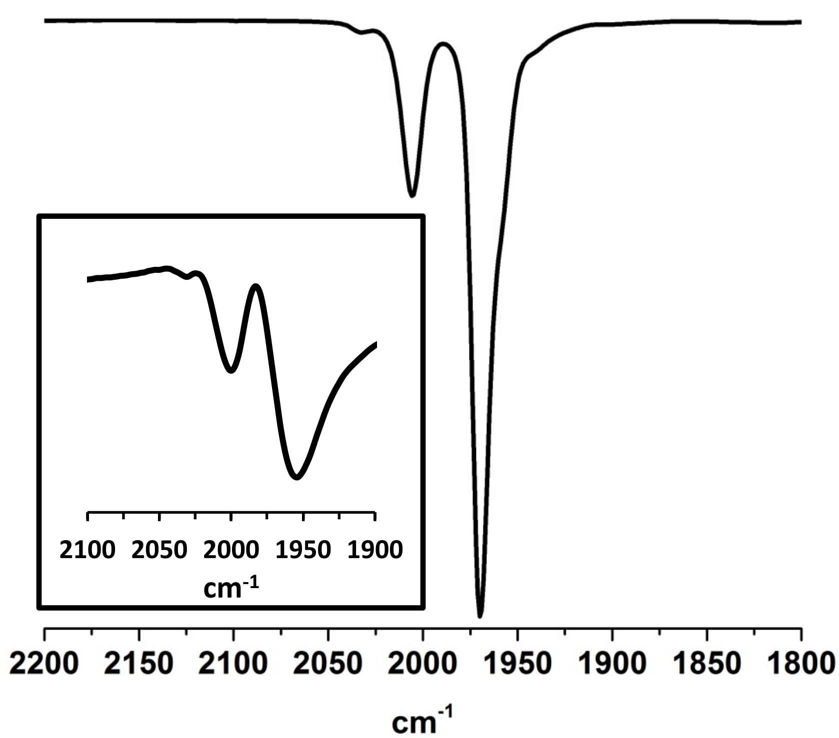

Figure S12. IR spectrum of Fe(pdt)$(CO)_2$(dppe) (**1d**) in THF solution and as a solid (inset).

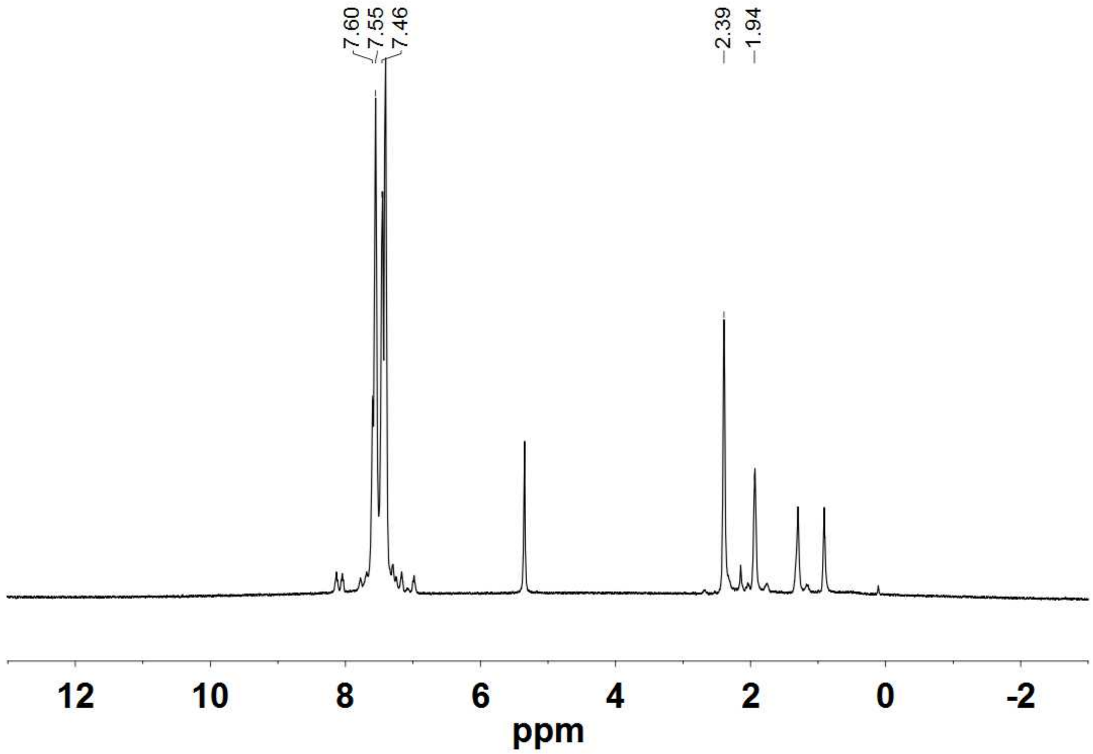

Figure S13. ^1H NMR spectrum (500 MHz) of $Fe(pdt)(CO)_2(dppbz)$ (**1e**) in CD_2Cl_2 solution.

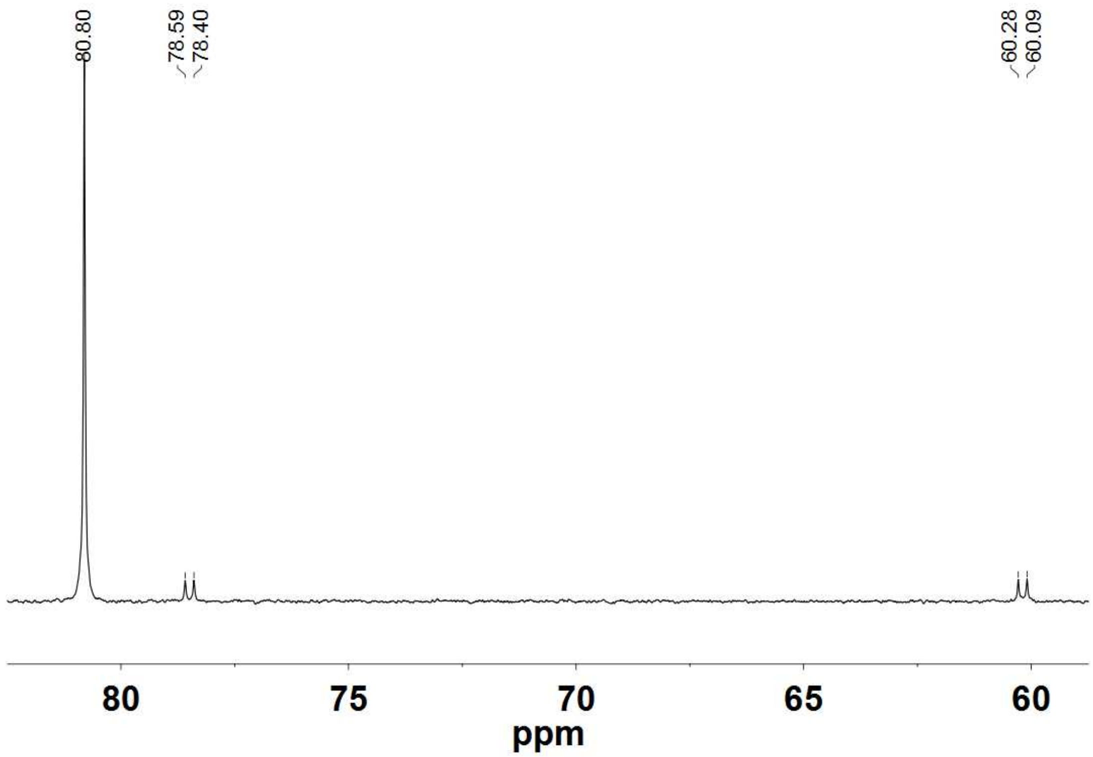

Figure S14. ^{31}P NMR spectrum (202 MHz) of Fe(pdt)(CO)$_2$(dppbz) (**1e**) in CD_2Cl_2 solution.

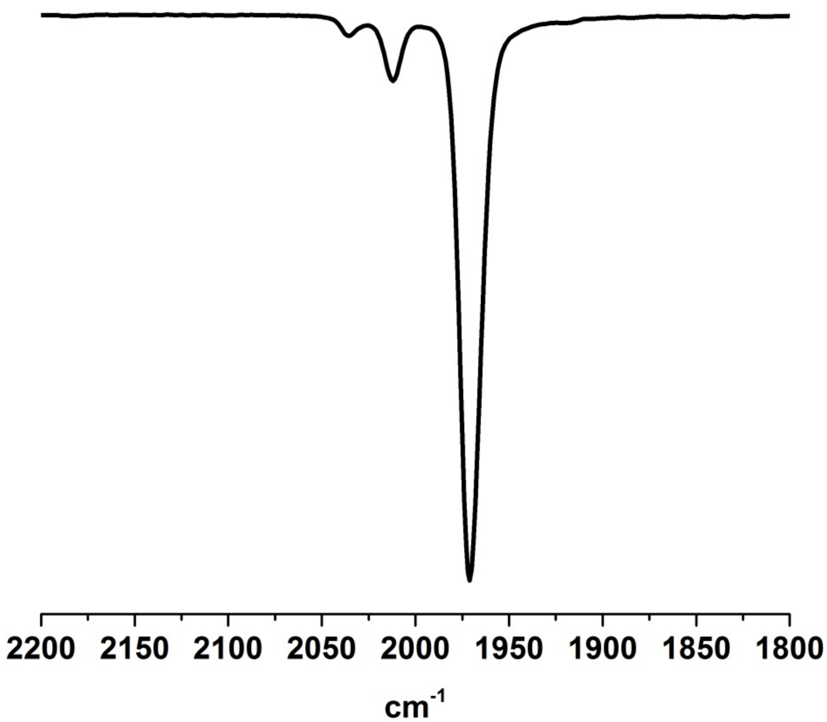

Figure S15. IR spectrum of Fe(pdt)(CO)$_2$(dppbz) (**1e**) in THF solution.

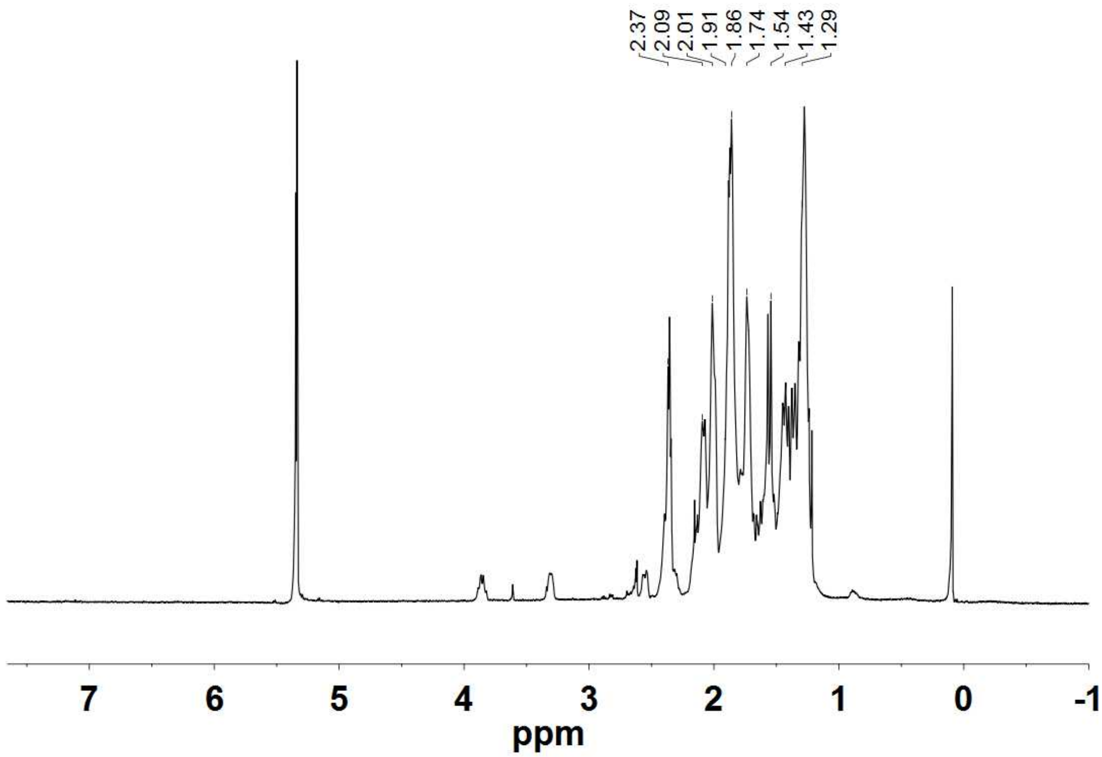

Figure S16. ^{1}H NMR spectrum (500 MHz) of Fe(pdt)$(CO)_2$(dcpe) (**1f**) in CD_2Cl_2 solution.

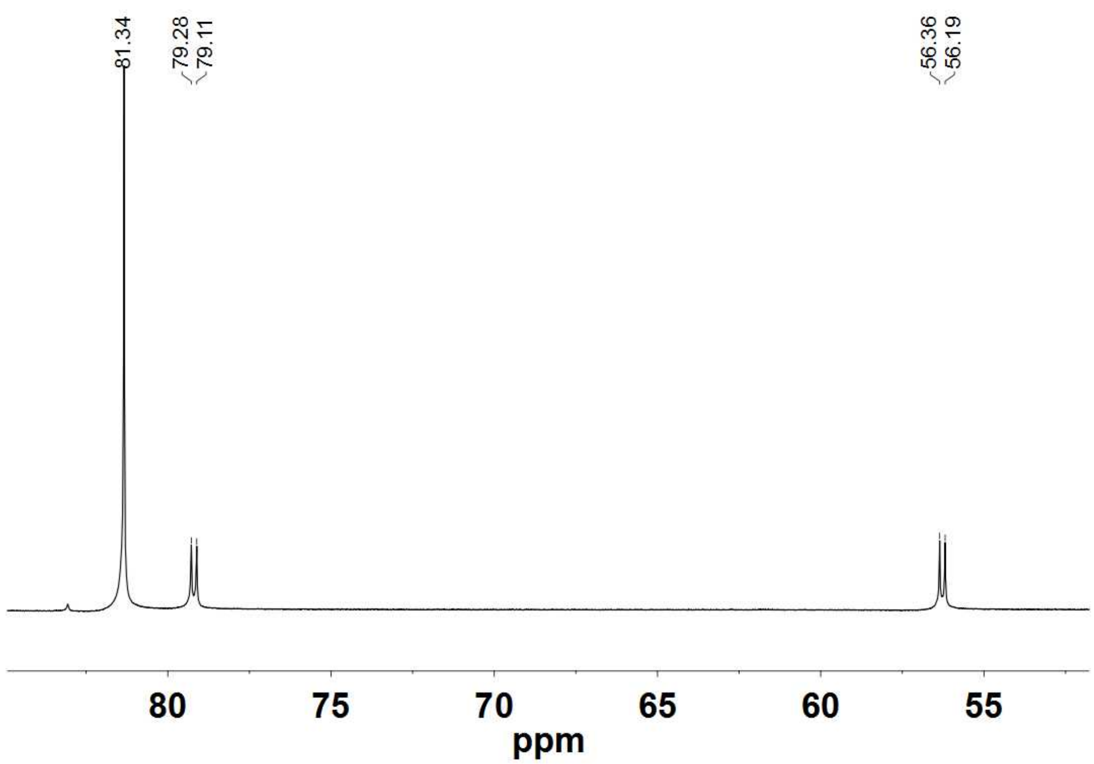

Figure S17. ^{31}P NMR spectrum (202 MHz) of Fe(pdt)$(CO)_2$(dcpe) (**1f**) in CD_2Cl_2 solution.

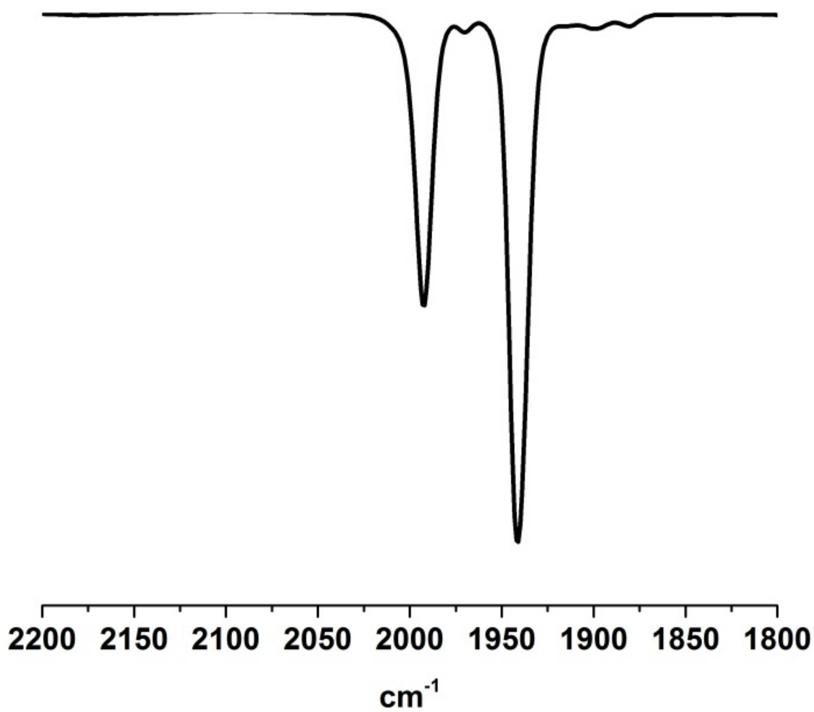

Figure S18. IR spectrum of Fe(pdt)$(CO)_2$(dcpe) (**1f**) in THF solution.

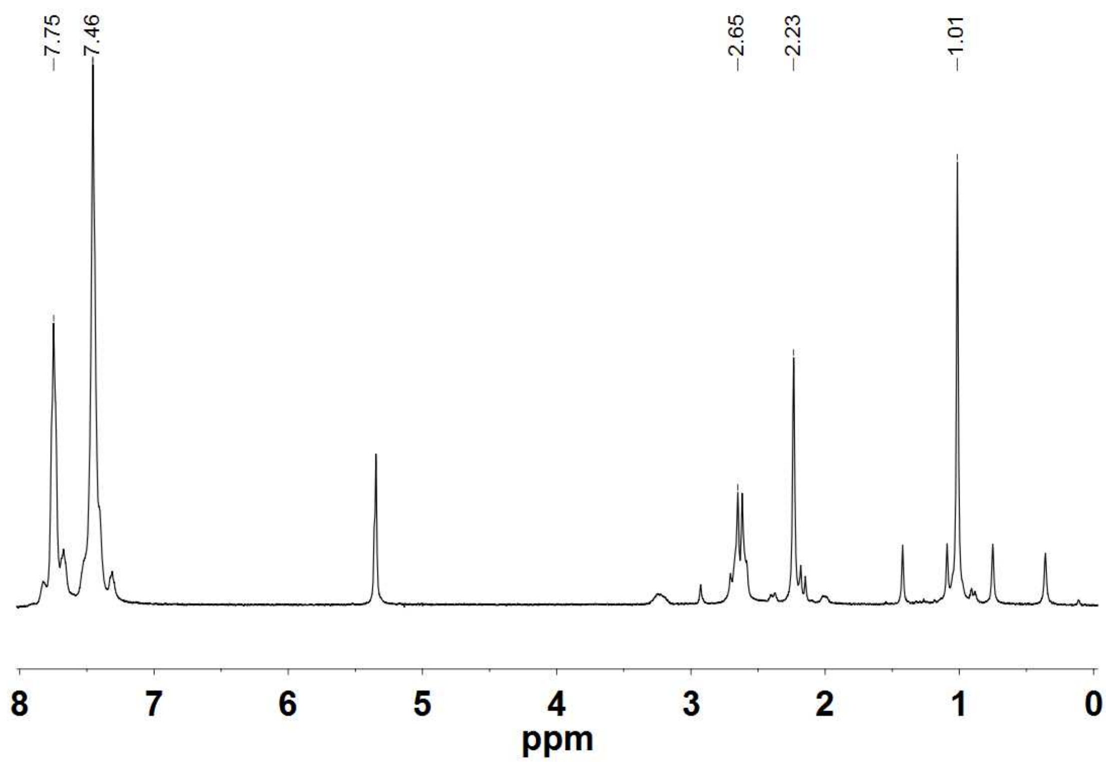

Figure S19. ^{1}H NMR spectrum (500 MHz) of $Fe(Me_2pdt)(CO)_2(dppe)$ (**1g**) in CD_2Cl_2 solution.

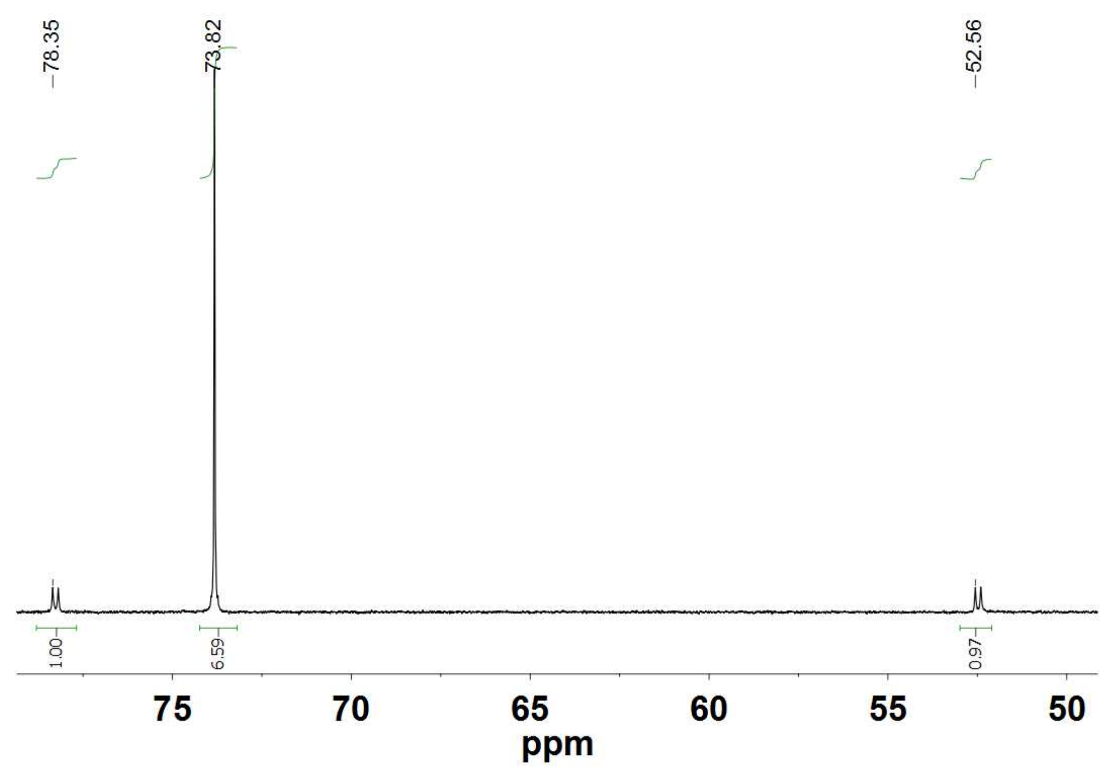

Figure S20. ^{31}P NMR spectrum (202 MHz) of $Fe(Me_2pdt)(CO)_2(dppe)$ (**1g**) in CD_2Cl_2 solution.

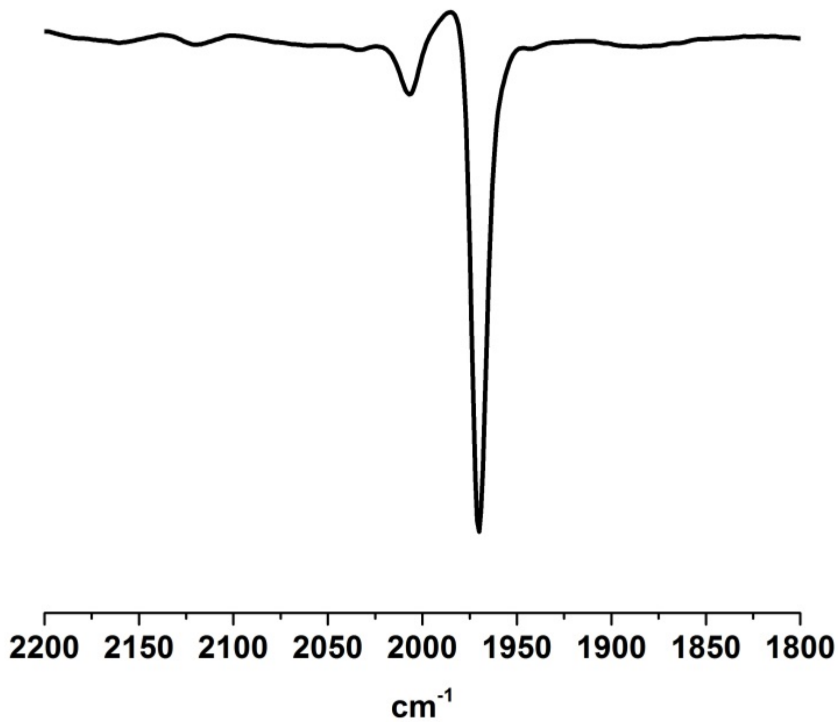

Figure S21. IR spectrum of $Fe(Me_2pdt)(CO)_2(dppe)$ (**1g**) in THF solution.

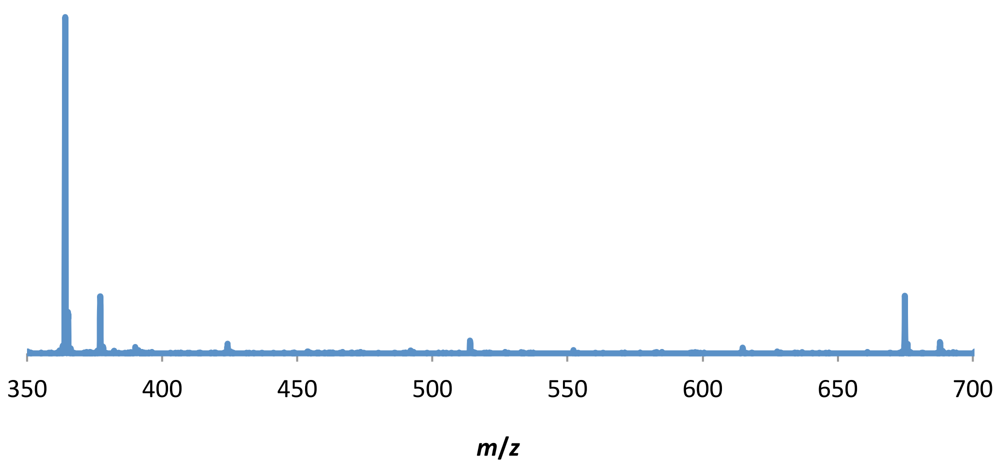

Figure S22. Positive ion ESI mass spectrum of $^{57}Fe_2I_4(^iPrOH)_4$.

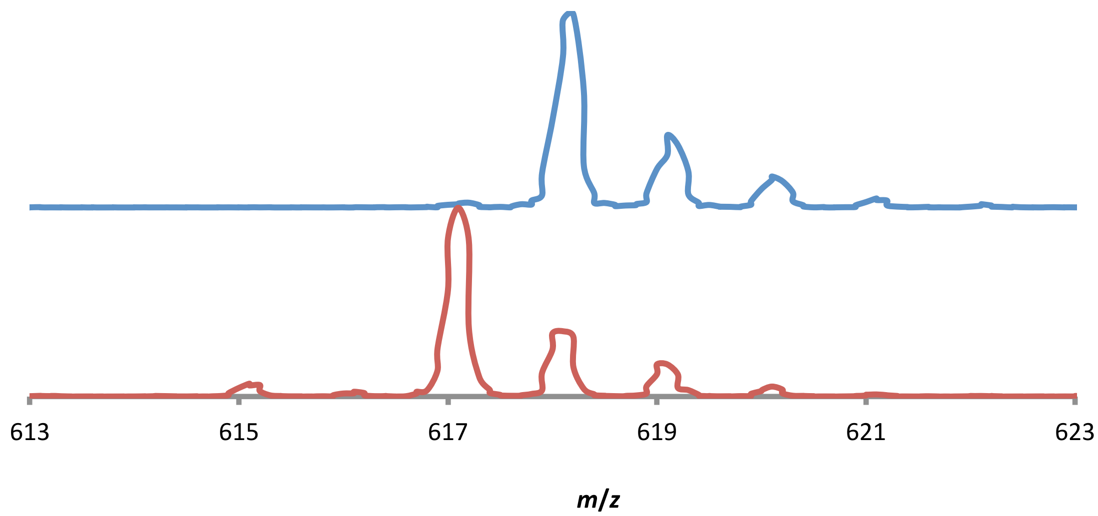

Figure S23. Positive ion ESI mass spectrum of *cis*/*trans*-[^{57}Fe(pdt)(CO)$_2$(dppe)] (**^{57}1d**, top) and *cis*/*trans*-[Fe(pdt)(CO)$_2$(dppe)] (**1d**, bottom) prepared using the same method.

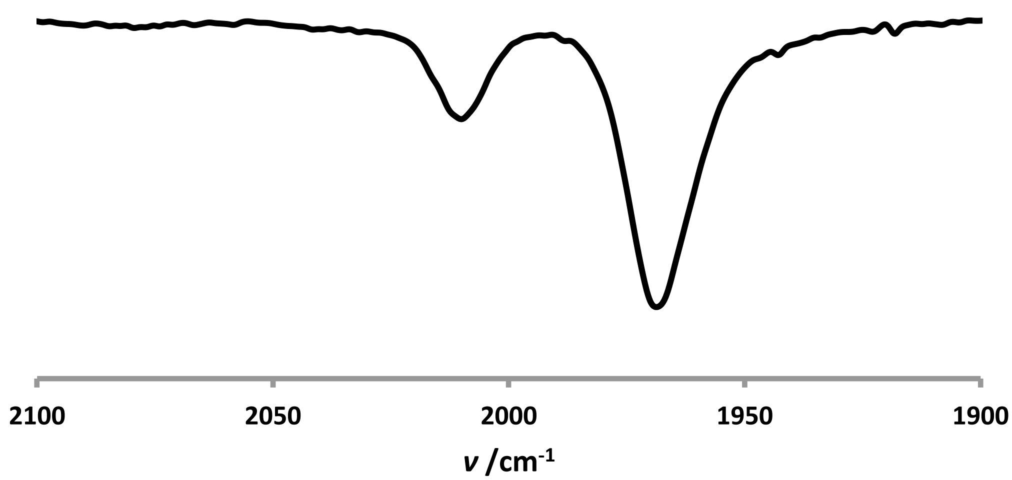

Figure S24. IR spectrum of *cis*/*trans*-[^{57}Fe(pdt)(CO)$_2$(dppe)] (**^{57}1d**) in CH_2Cl_2 solution.

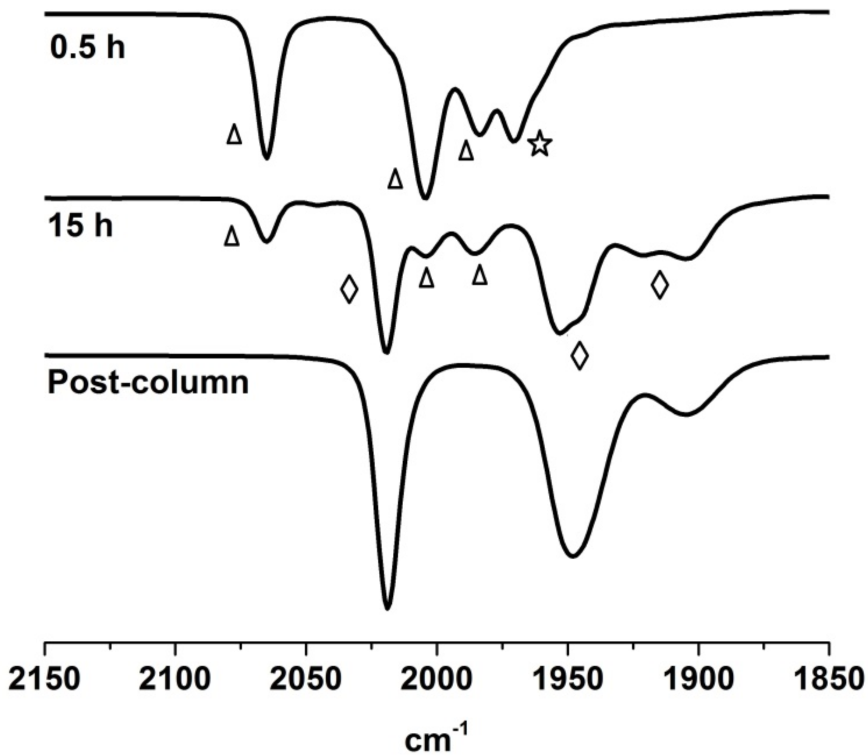

Figure S25. IR spectra of two stages in the reaction (bda)Fe$(CO)_3$ (triangle) + Fe(pdt)$(CO)_2$(dppe) (**1d**) (star), and the purified Fe_2(pdt)$(CO)_4$(dppe) (**2d**) (diamond).

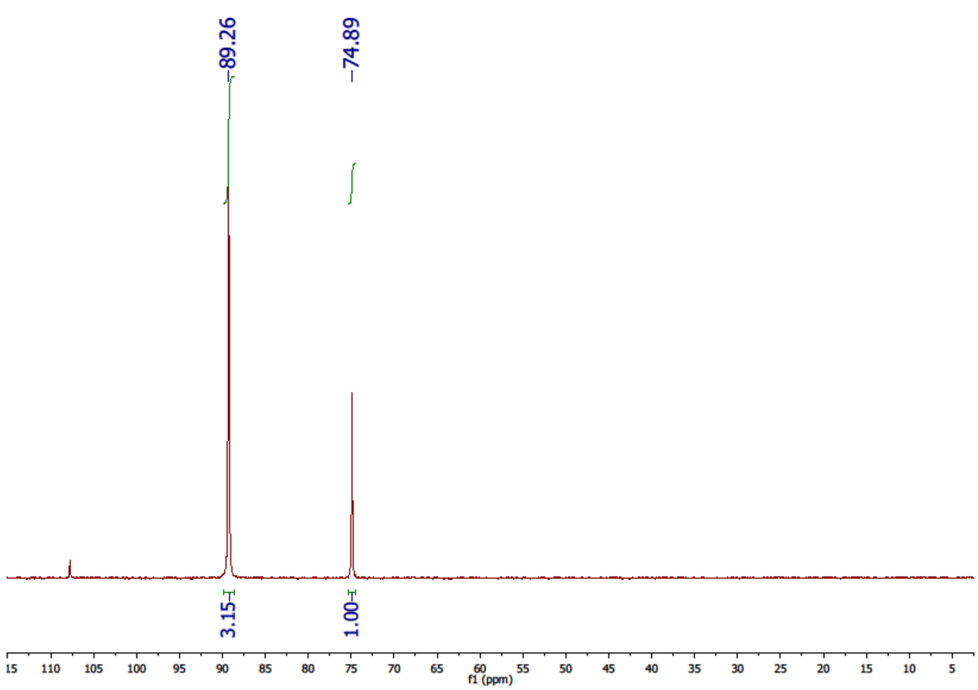

Figure S26. ^{31}P NMR spectrum of Fe_2(pdt)(dcpe)$(CO)_4$ (**2f**) in CD_2Cl_2. Signal at 107 is impurity present as less than 2%.

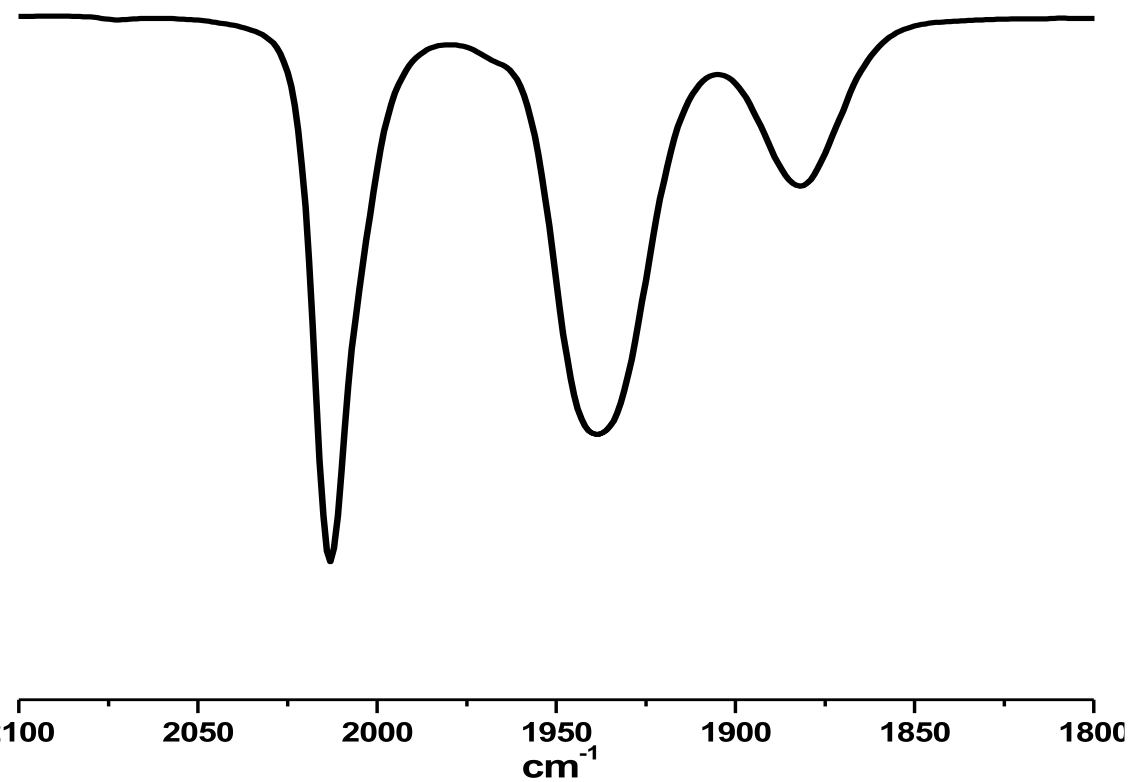

Figure S27. IR spectra of purified $Fe_2(pdt)(CO)_4(dcpe)$ (**2f**) in CH_2Cl_2.

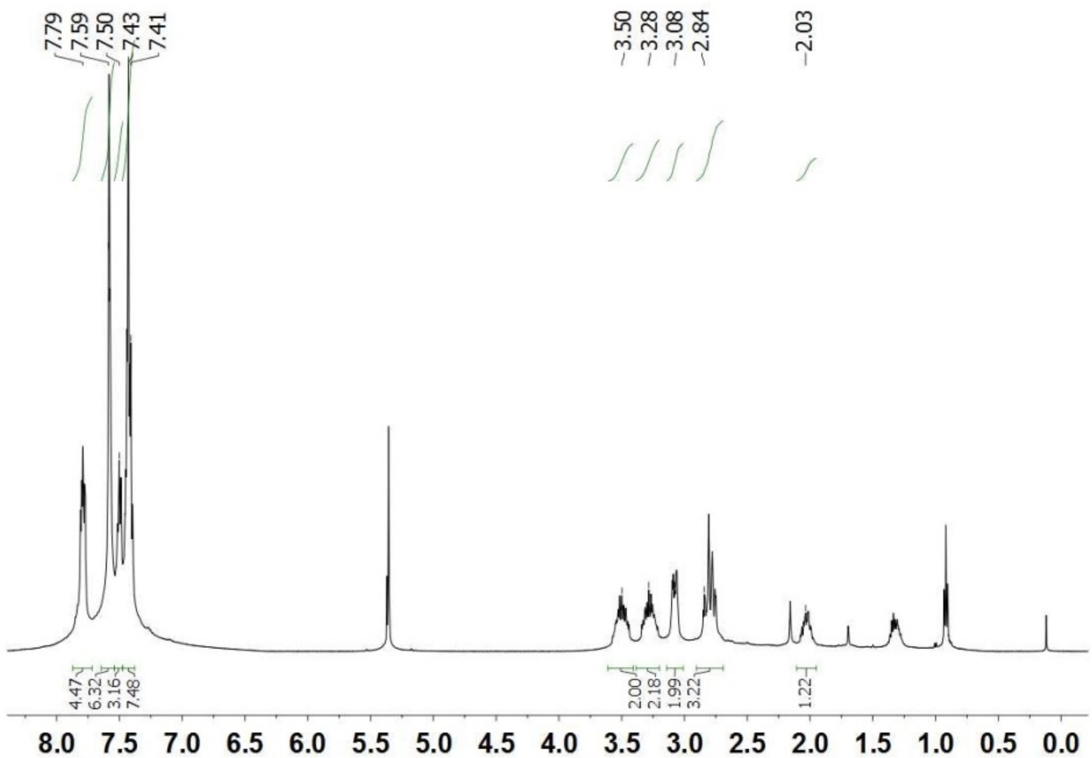

Figure S28. ^{1}H NMR spectrum of $[(CO)_3Mn(pdt)Fe(CO)_2(dppe)]BF_4$ ([**3d**(CO)]BF_4) in CD_2Cl_2.

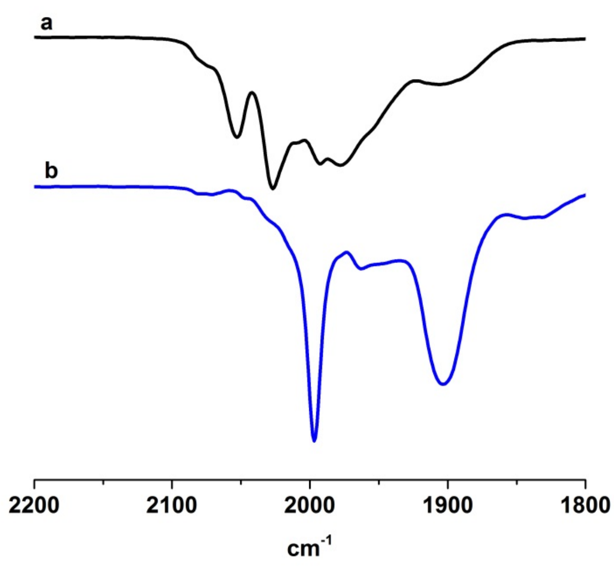

Figure S29. IR spectrum of (a) $[(CO)_3Mn(pdt)Fe(CO)_2(dppe)]BF_4$ ([**3d**(CO)]BF_4) at 25 °C and (b) $(CO)_3Mn(pdt)Fe(CO)(dppe)$ (**3d**) at -78 °C in CH_2Cl_2.

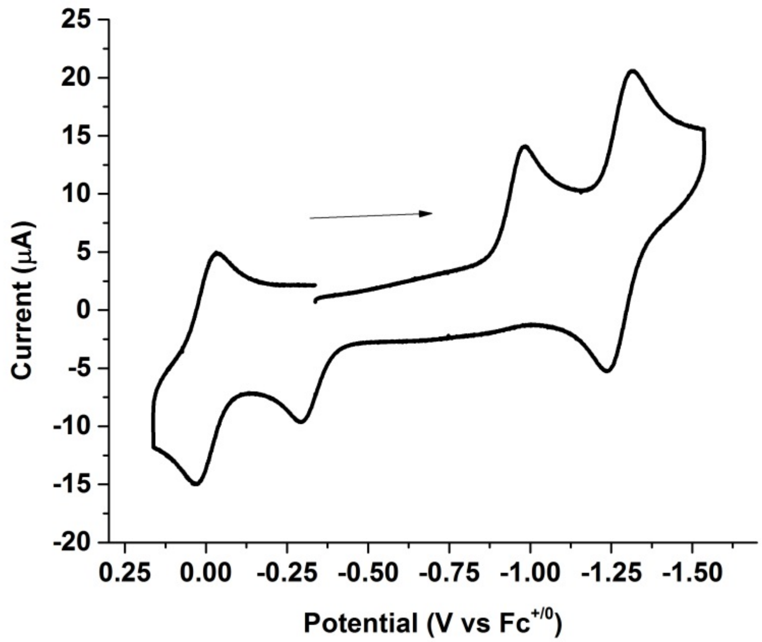

Figure S30. Cyclic voltammogram of 1.0 mM [(CO)$_3$Mn(pdt)Fe(CO)$_2$(dppe)]BF$_4$ ([**3d**(CO)]BF$_4$) in CH_2Cl_2 at 25 °C. Conditions are described in the caption for Figure S42 but in this experiment, the scan rate was 1.0 V/s.

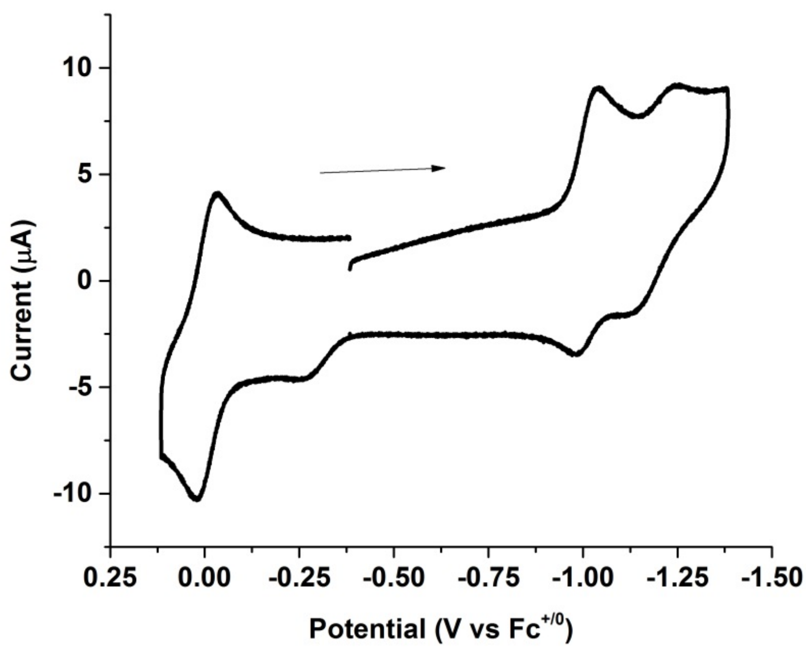

Figure S31. Cyclic voltammogram of 1.0 mM [(CO)$_3$Mn(pdt)Fe(CO)$_2$(dppe)]BF$_4$ ([**3d**(CO)]BF$_4$) in CH_2Cl_2 at −78 °C. Conditions are described in the caption for Figure S42.

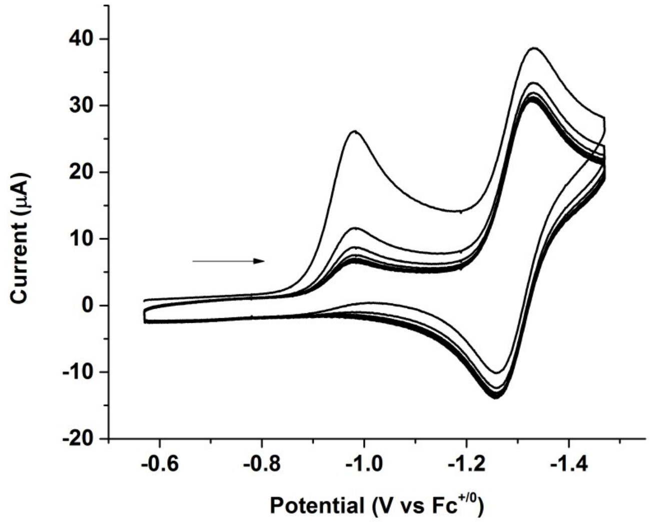

Figure S32. Cyclic voltammogram of $[(CO)_3Mn(pdt)Fe(CO)_2(dppe)]BF_4$ in CH_2Cl_2, scanning 20 segments without disturbing the solution or polishing the working electrode.
Conditions are described in the caption for Figure S42 but in this experiment, the scan rate was 1.0 V/s.

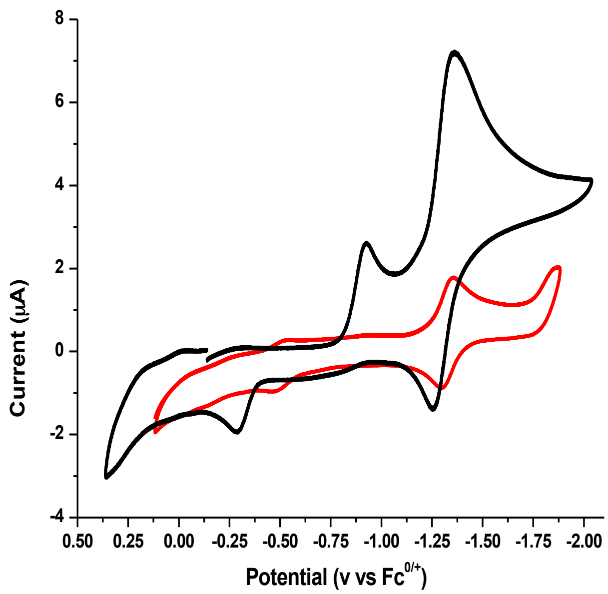

Figure S33. Black trace: Cyclic voltammogram of 1.0 mM $[(CO)_3Mn(pdt)Fe(CO)_2(dppe)]BF_4$ ([**3d**(CO)]BF_4) in THF at 25 °C. Red Trace: Cyclic voltammogram of 1.0 mM $(CO)_3Mn(pdt)Fe(CO)(dppe)$ under identical conditions.
Conditions: see Figure S42.

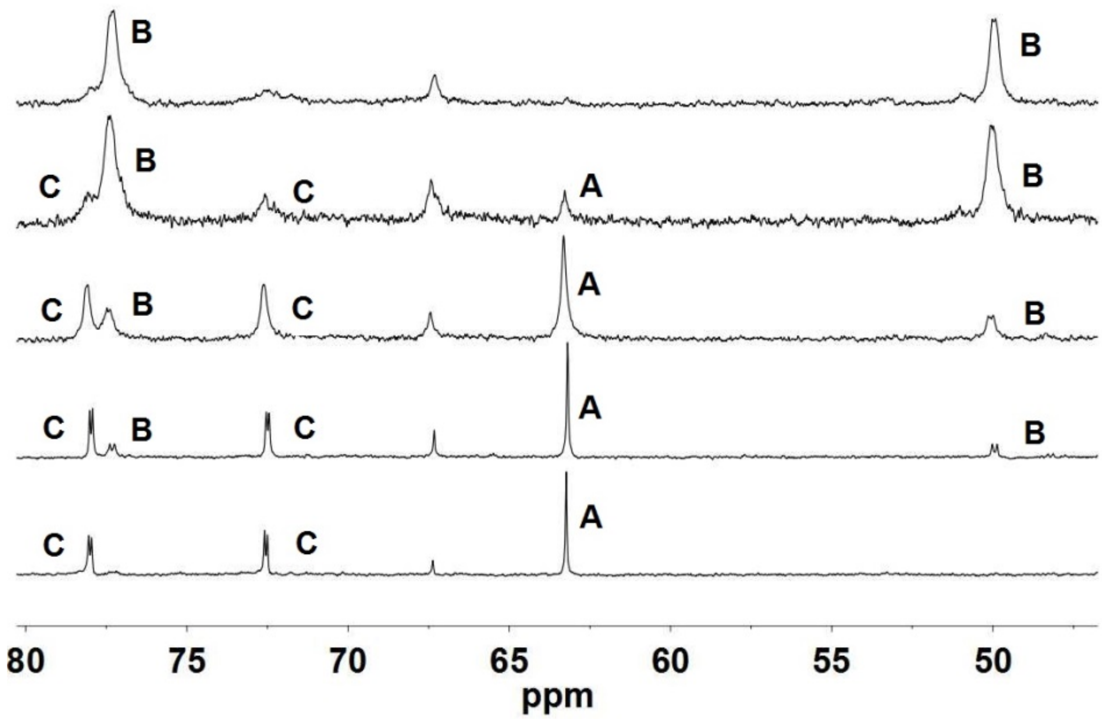

Figure S34. ^{31}P NMR spectra for stages in the reaction of a 1:1 mixture of [(acenapthene)Mn(CO)$_3$]BF$_4$ with Fe(edt)(CO)$_2$(dppe) (**1b**) in CD$_2$Cl$_2$ solution at 20 °C. From top to bottom reaction time = 15 min, 3.5 h, 30 h, 48 h, 3 weeks). Proposed reaction pathway and isomer assignments are shown below.

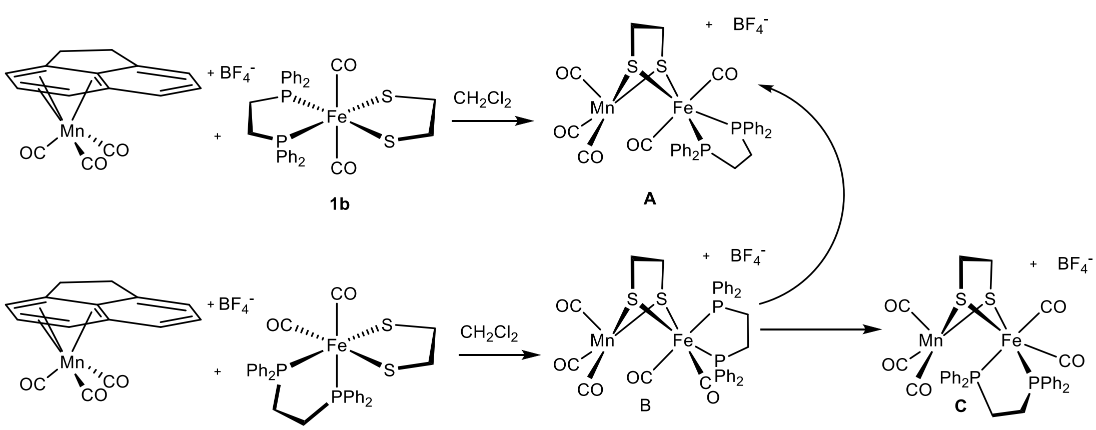

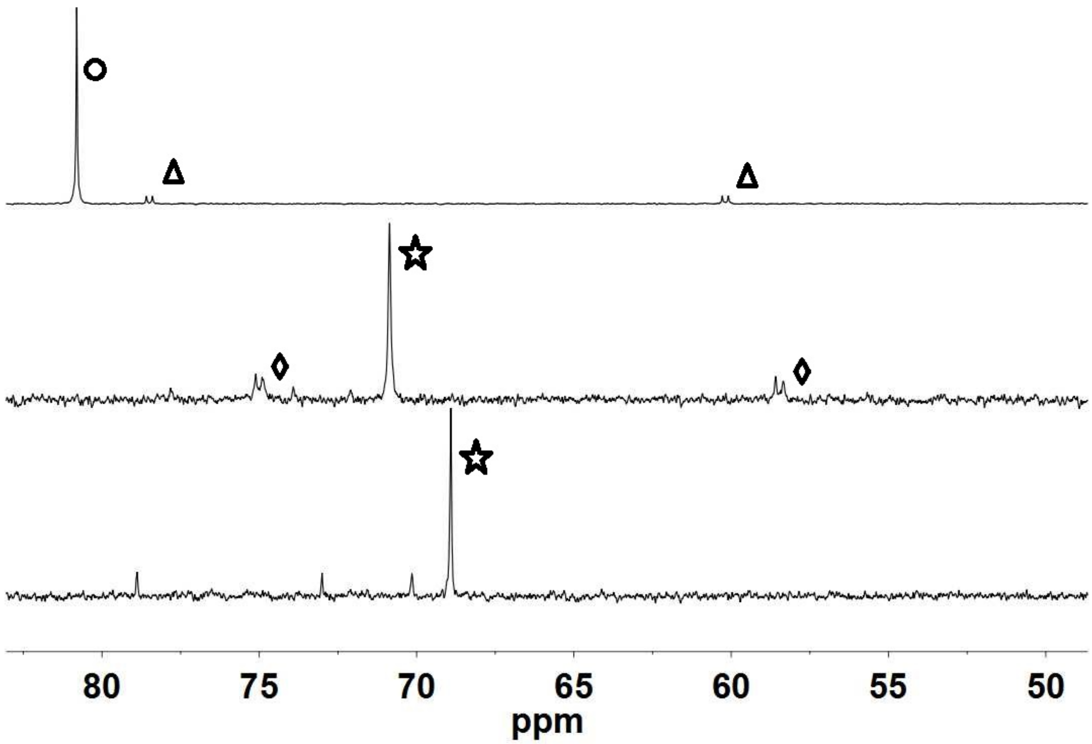

Figure S35. ^{31}P NMR spectra related to the reaction of Fe(pdt)(CO)$_2$(dppbz) (**1e**) and [(acenaphthene)Mn(CO)$_3$]BF$_4$ to give [(CO)$_4$Mn(pdt)Fe(CO)(dppbz)]BF$_4$ (CD_2Cl_2 solutions):

Top: unsym-**1e** (triangle) and *sym*-**1e** (circle).

Middle: **1e** + [(acenaphthene)Mn(CO)$_3$]BF$_4$ after 3 h (diamond = *unsym*-[(CO)$_4$Mn(pdt)Fe(CO)(dppbz)]$^+$, star = *sym*-[(CO)$_4$Mn(pdt)Fe(CO)(dppbz)]$^+$)

Bottom: Same mixture was allowed to stand 12 h, evaporated and recrystallized from CH_2Cl_2/hexanes (signals at δ 73.1 and 70.2 are unknown impurities).

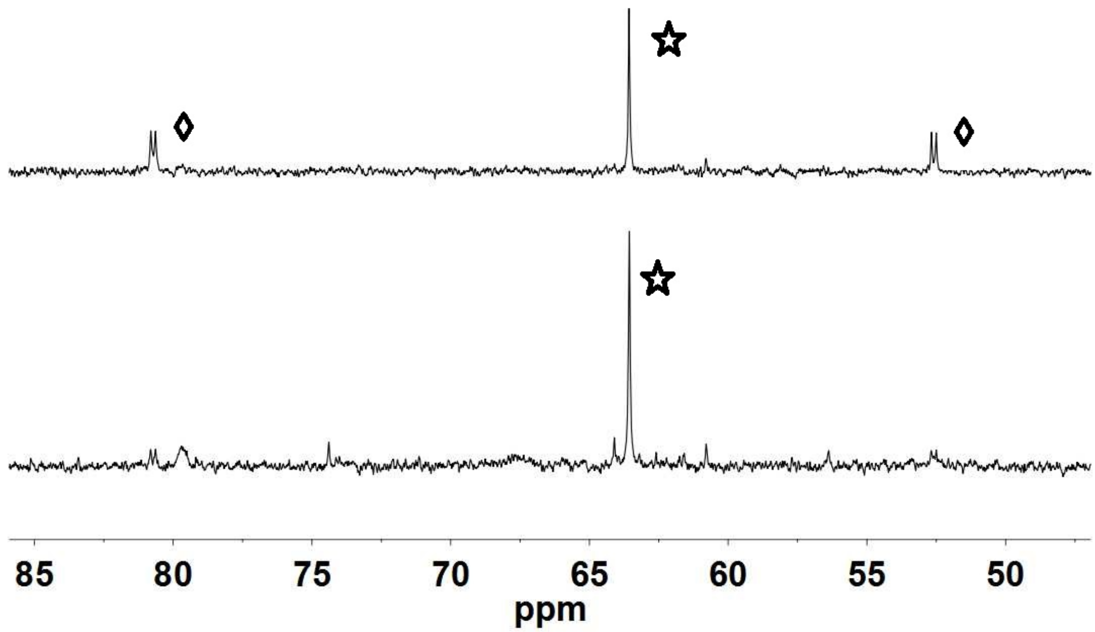

Figure S36. ^{31}P NMR spectra related to the reaction of Fe(pdt)(CO)$_2$(dcpe) (**1f**) and [(acenaphthene)Mn(CO)$_3$]BF$_4$ to give [(CO)$_4$Mn(pdt)Fe(CO)(dcpe)]BF$_4$ (CD$_2$Cl$_2$ solutions):
Top: unsym-**1f** (diamonds) and *sym*-**1f** (stars).
Bottom: **1f** + [(acenaphthene)Mn(CO)$_3$]BF$_4$ after 16 h.

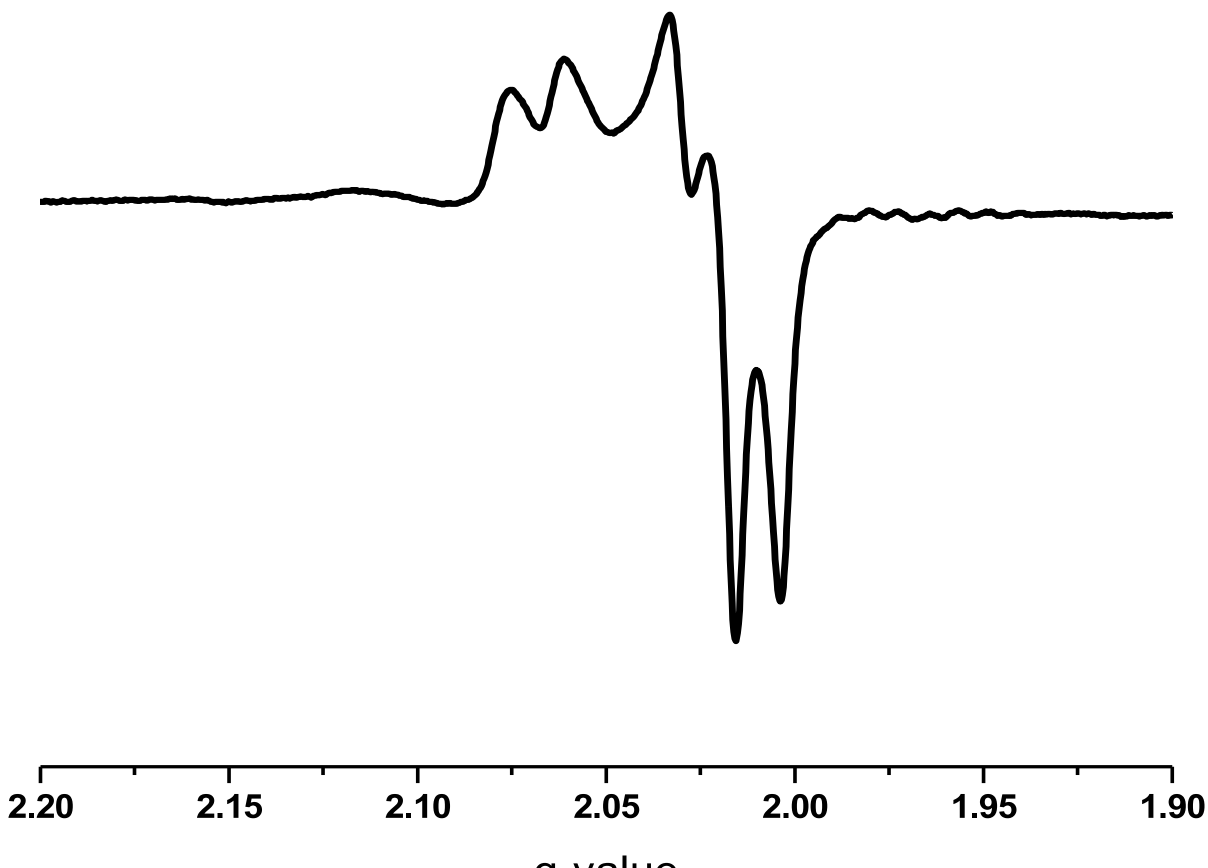

Figure S37. X-band EPR spectra of a mixture of $[(CO)_3Mn(pdt)Fe(CO)_2(dppe)]BF_4$ ([**3d**(CO)]BF_4) and Cp_2Co in 4:1 mixture of THF and toluene frozen at 77 K.

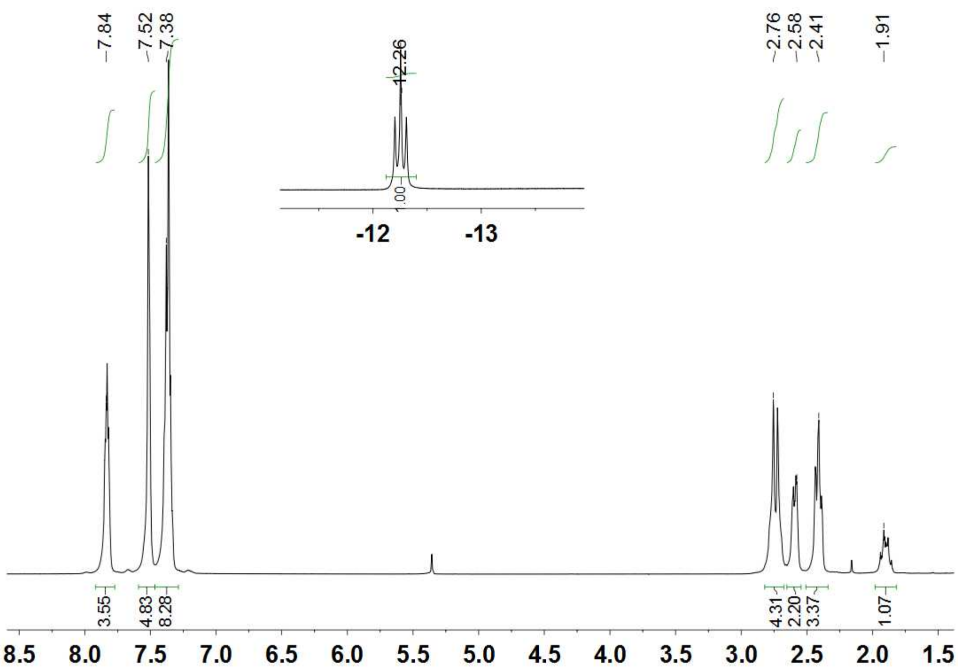

Figure S38. ^{1}H NMR spectrum of $(CO)_3Mn(pdt)(\mu\text{-}H)Fe(CO)(dppe)$ (H**3d**) in CD_2Cl_2 solution (*Inset:* High field region of spectrum, showing signal for the hydride ligand).

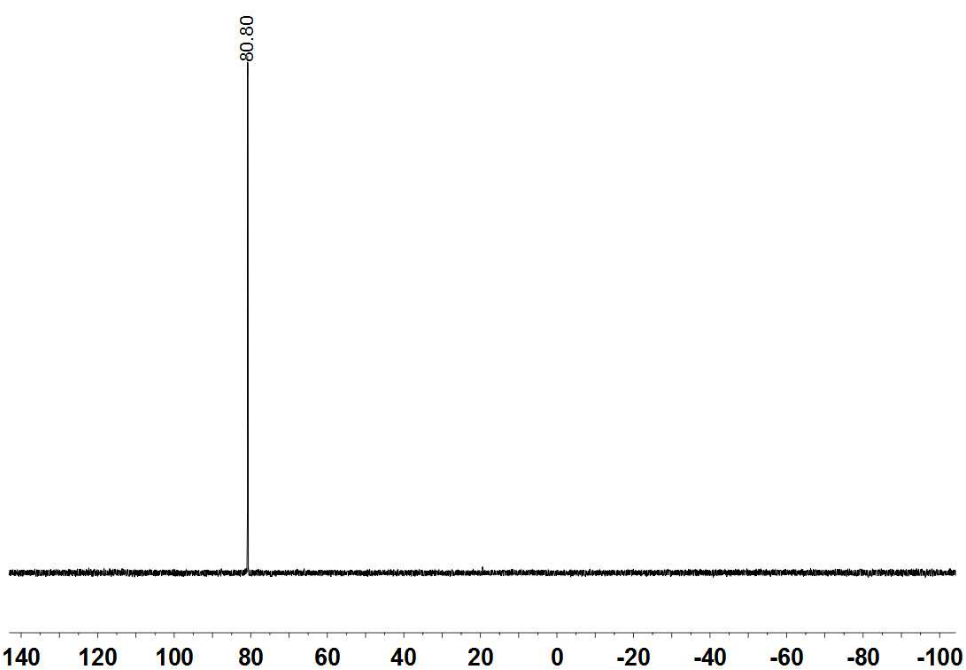

Figure S39. ^{31}P NMR spectrum of $(CO)_3Mn(pdt)(\mu\text{-}H)Fe(CO)(dppe)$ (H**3d**) in CD_2Cl_2 solution.

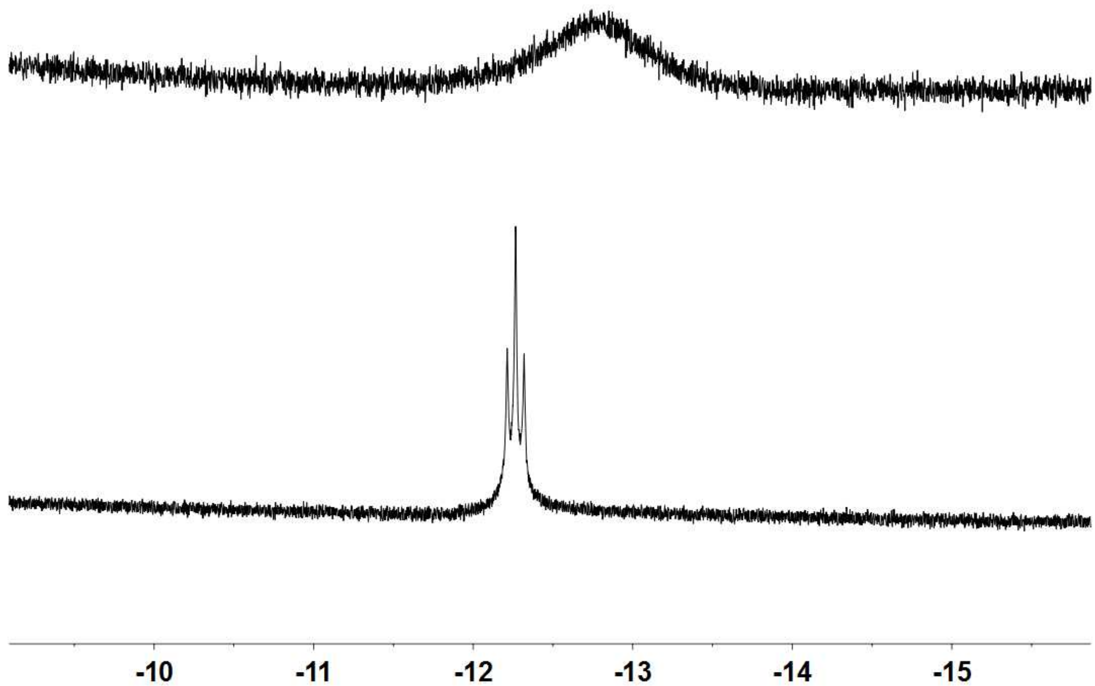

Figure S40. High field region of the ^{1}H NMR spectra of H**3d** (bottom) and a 1:1 mixture of H**3** and $[H(Et_2O)_2]BAr^F_{24}$ (top) in CH_2Cl_2 solution.

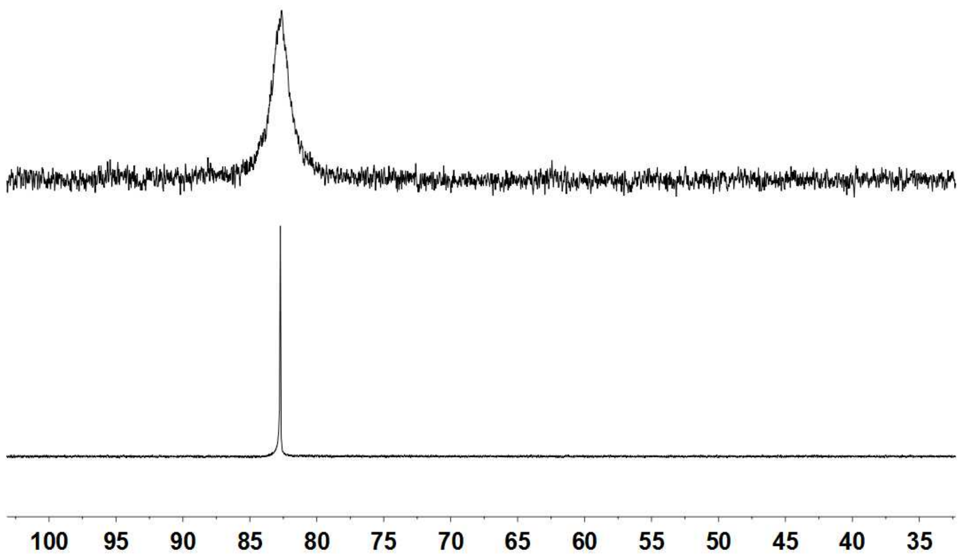

Figure S41. ^{31}P NMR spectra of H**3d** (bottom) and of a 1:1 mixture of H**3d** and $[H(Et_2O)_2]BAr^F{}_{24}$ (top) in CH_2Cl_2 solution.

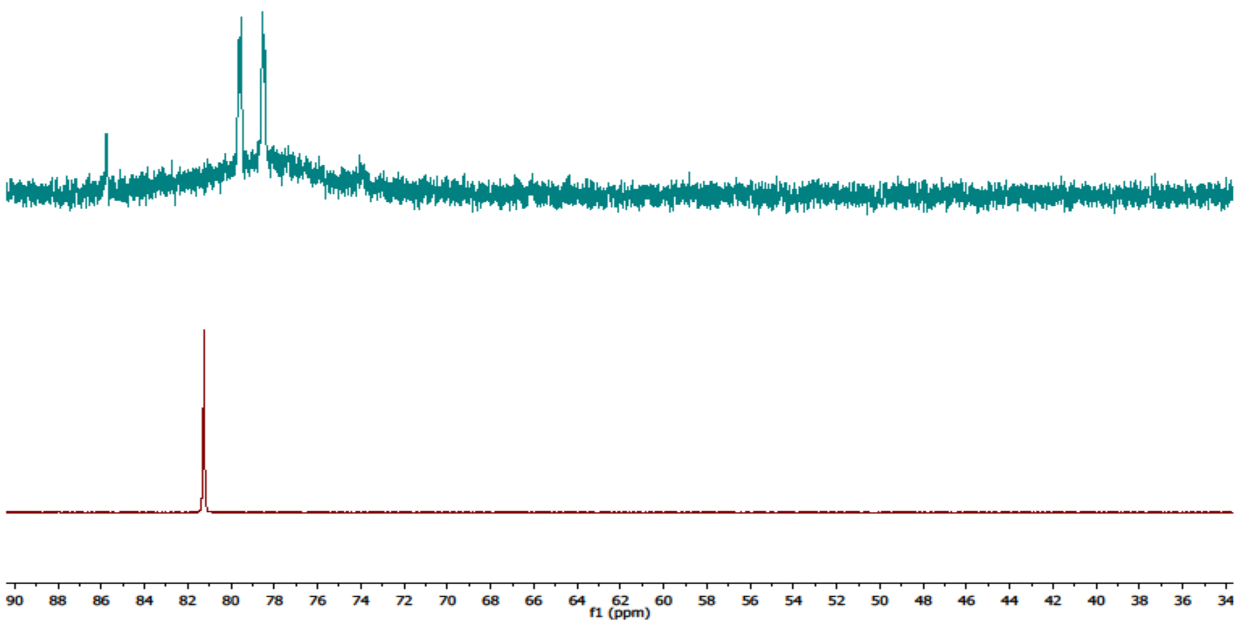

Figure S42. ^{31}P NMR spectra of H**3** (bottom) and of a 1:2 mixture of H**3d** and $[H(Et_2O)_2]BAr^F{}_{24}$ (top). For the top spectrum, $J_{P\text{-}P}$ is 21.5 Hz. The signal at δ86 is an unidentified impurity. *Note:* When the protonation was conducted under an atmosphere of CO, however, the IR spectrum of the reaction mixture did not indicate formation of [**3**(CO)]$^+$.

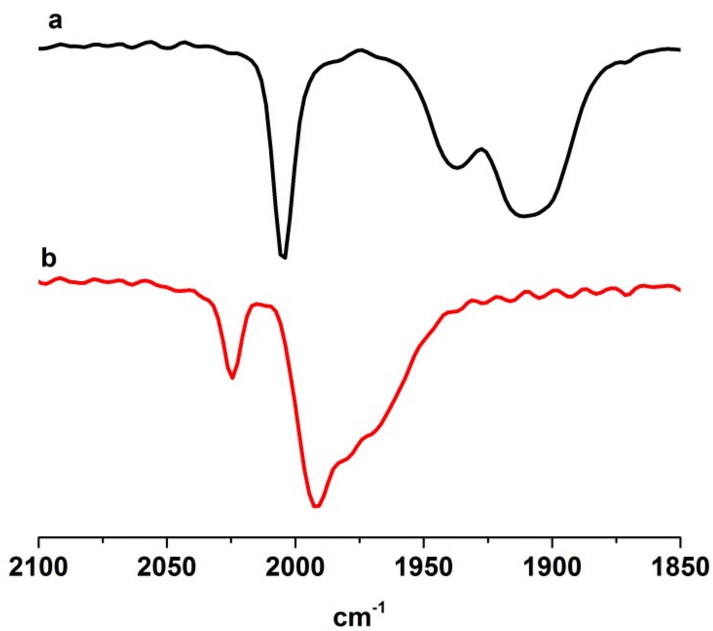

Figure S43. IR spectra of CH_2Cl_2 solutions of (a) $(CO)_3Mn(pdt)(\mu\text{-}H)Fe(CO)(dppe)$ (H**3d**) before and after treatment with $FcBF_4$.

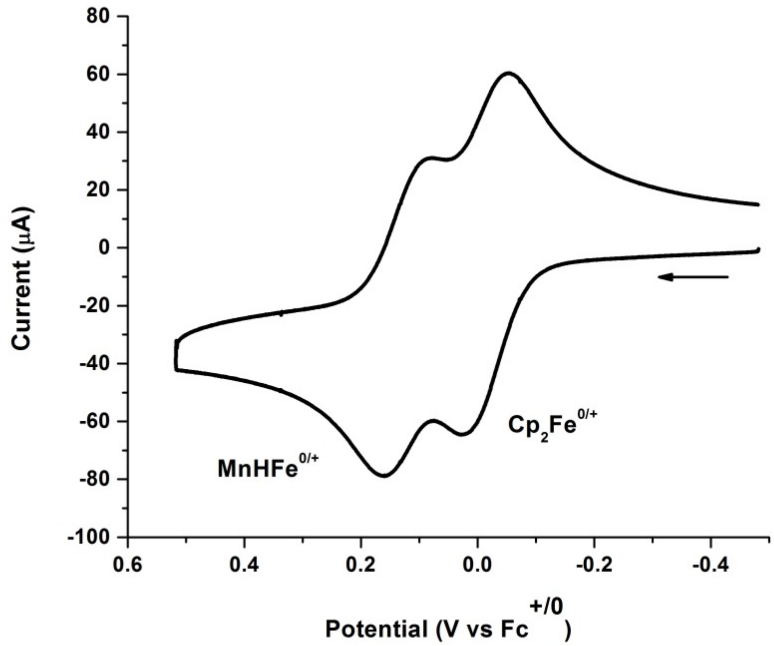

Figure S44. Cyclic voltammogram of $(CO)_3Mn(pdt)(\mu\text{-}H)Fe(CO)(dppe)$ (H**3d**) in CH_2Cl_2 solution. *Conditions:*
1.0 mM $(CO)_3Mn(pdt)(\mu\text{-}H)Fe(CO)(dppe)$
0.1 M $[Bu_4N]PF_6$
working electrode: glassy carbon
counter electrode: Pt
pseudoreference electrode: Ag
scan rate = 0.5 V/s

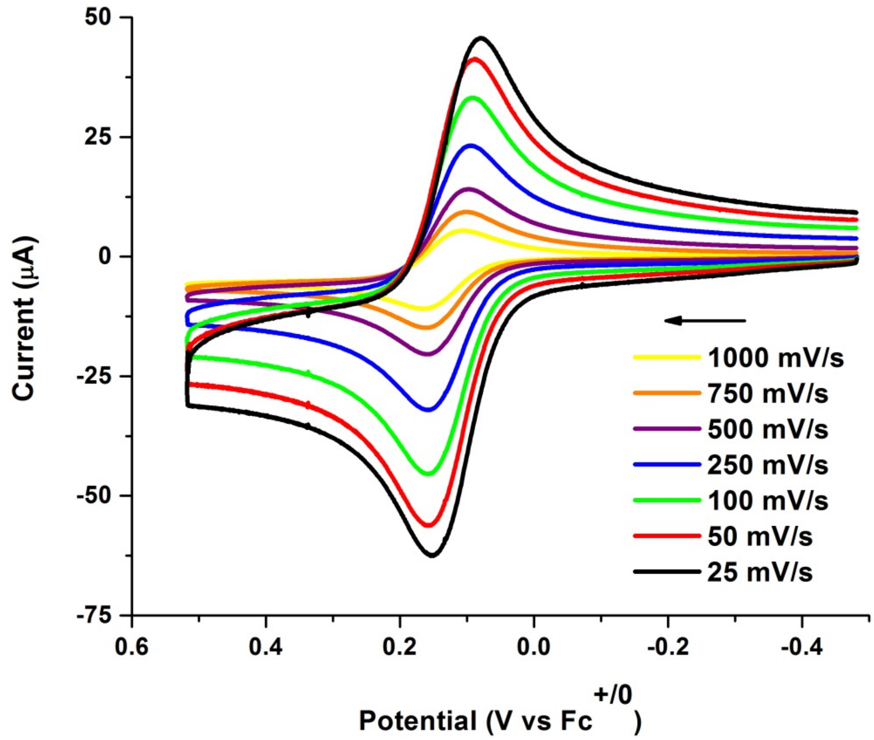

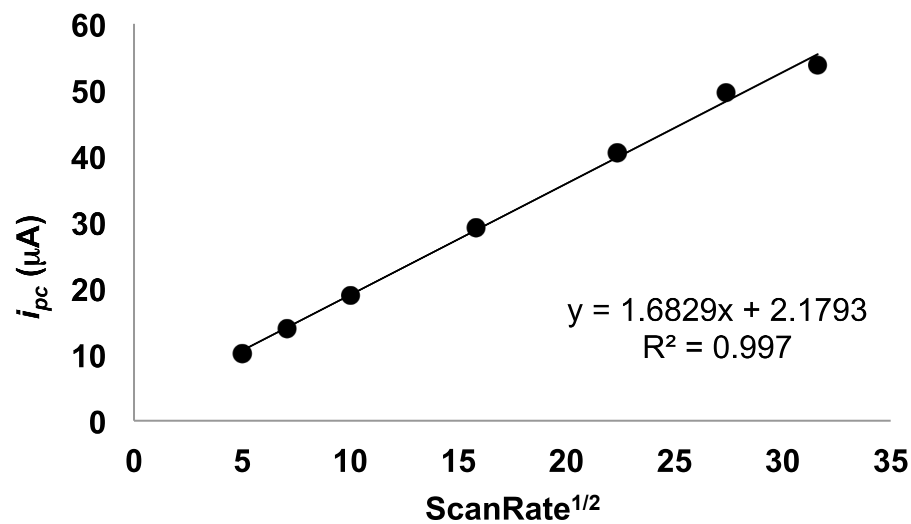

Figure S45. Cyclic voltammograms of $(CO)_3$Mn(pdt)(*μ*-H)Fe(CO)(dppe) (H**3d**) at various scan rates (top) and plot of i_{pc}/(scan rate)$^{1/2}$ (bottom).
Conditions: See Figure S42.

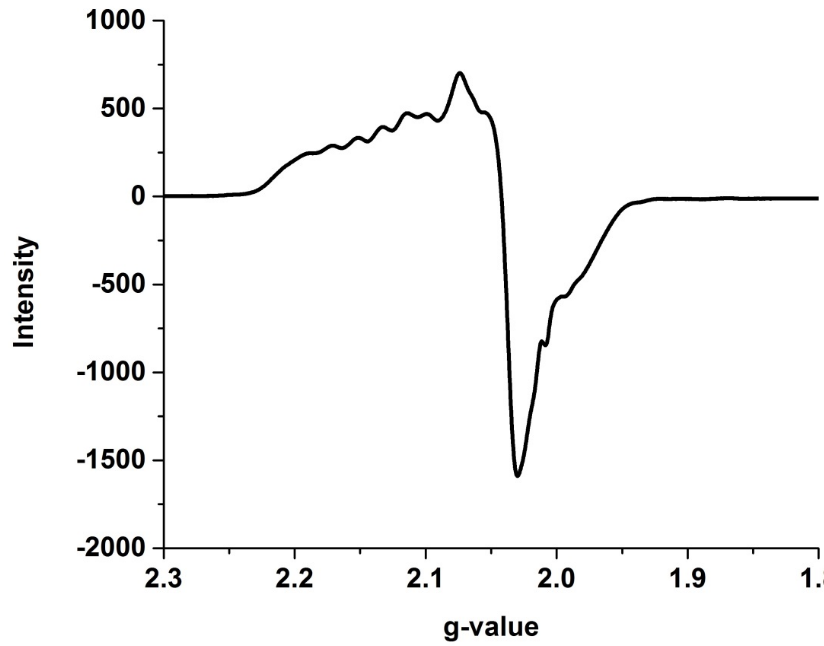

Figure S46. X-band EPR spectrum of a frozen (110 K) mixture of $(CO)_3Mn(pdt)(\mu\text{-}H)Fe(CO)(dppe)$ (H**3**) and [acetylFc]BAr^F_{24} in 3:1 toluene:CH_2Cl_2 solution.

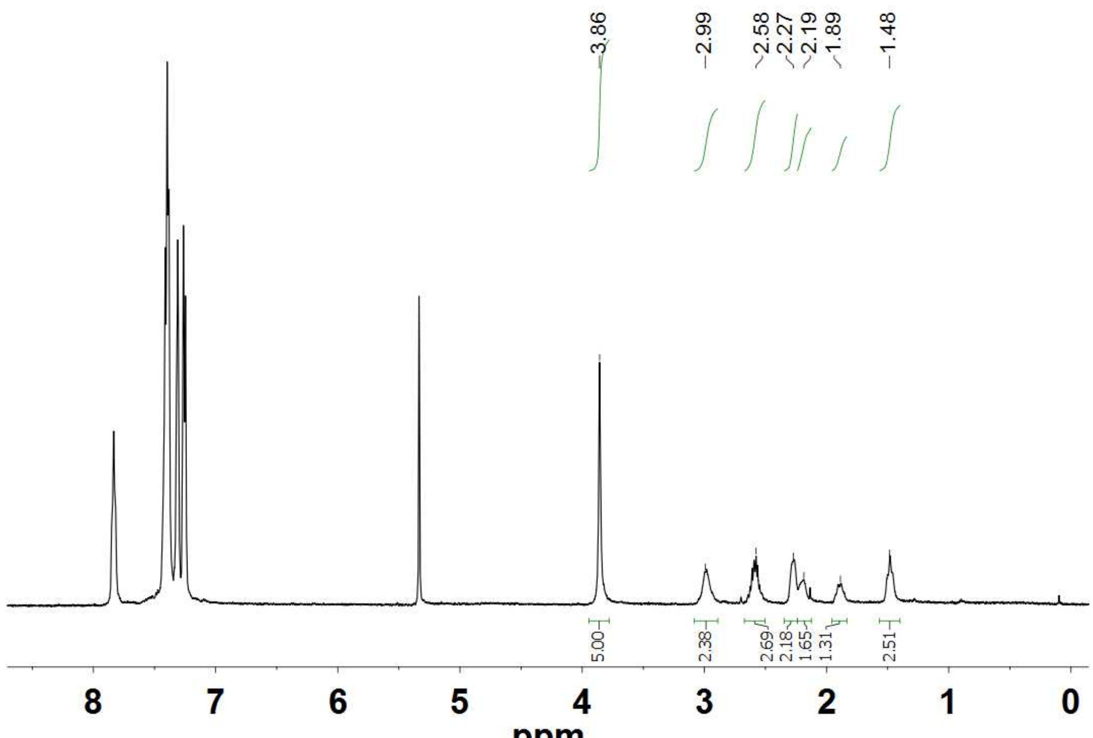

Figure S47. ^1H NMR spectrum of CpCo(pdt)Fe(CO)(dppe) (**4d**) in CD_2Cl_2 solution.

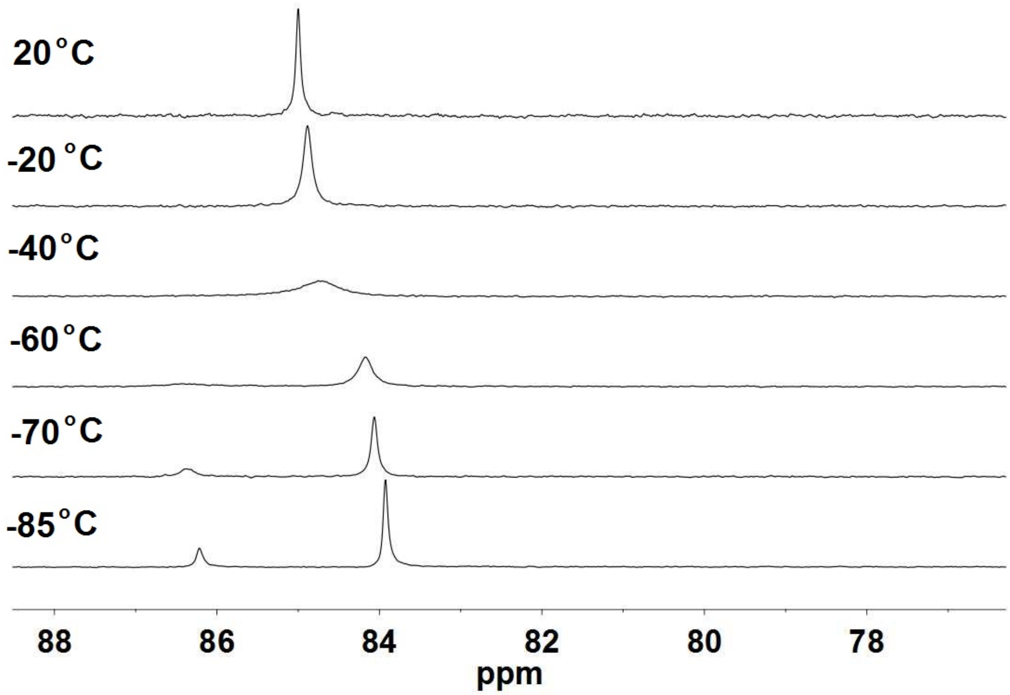

Figure S48. ^{31}P NMR spectrum of CpCo(pdt)Fe(CO)(dppe) (**4d**) in CD_2Cl_2 solution at various temperatures.

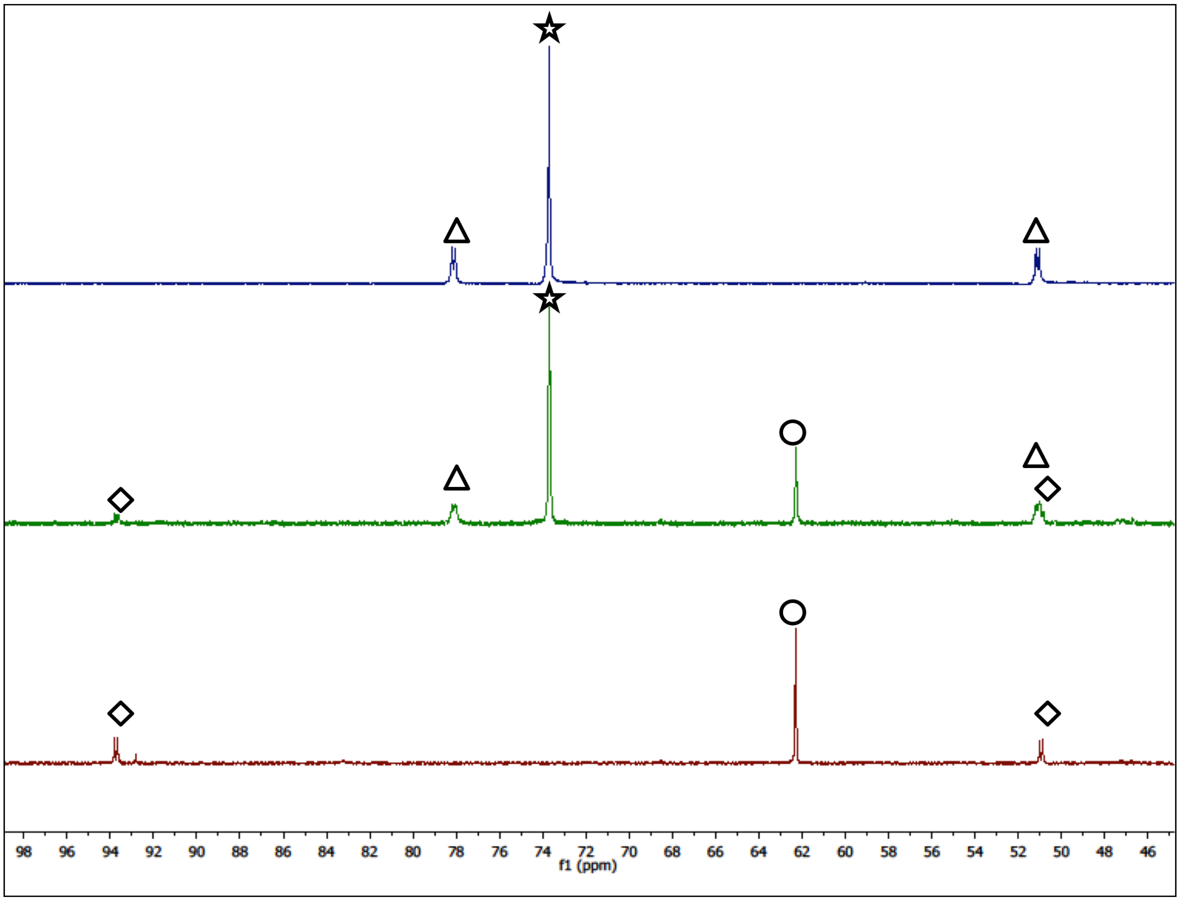

Figure S49. ^{31}P NMR spectra related to the reaction of Fe(pdt)(CO)$_2$(dppe) (**1d**) and CpCo(CO)I$_2$ to give [CpCoI(pdt)Fe(CO)(dppe)]I (CD$_2$Cl$_2$ solutions):
Top: *unsym*-**1d** (triangle) and *sym*-**1d** (star).
Middle: **1d** + CpCo(CO)I$_2$ after 30 min. (diamond = *unsym*-[CpCoI(pdt)Fe(CO)(dppe)]$^+$, circle = *sym*-[CpCoI(pdt)Fe(CO)(dppe)]$^+$).
Bottom: Same mixture as in middle spectrum, but recorded after a total of 100 min.

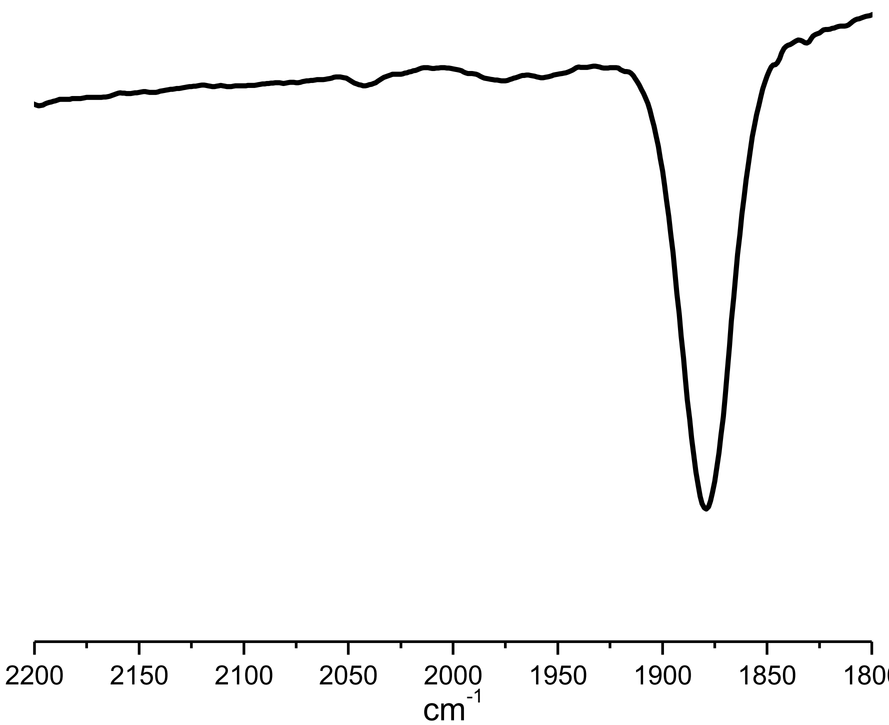

Figure S50. IR spectrum of CpCo(pdt)Fe(CO)(dppe) (**4d**) in CH_2Cl_2.

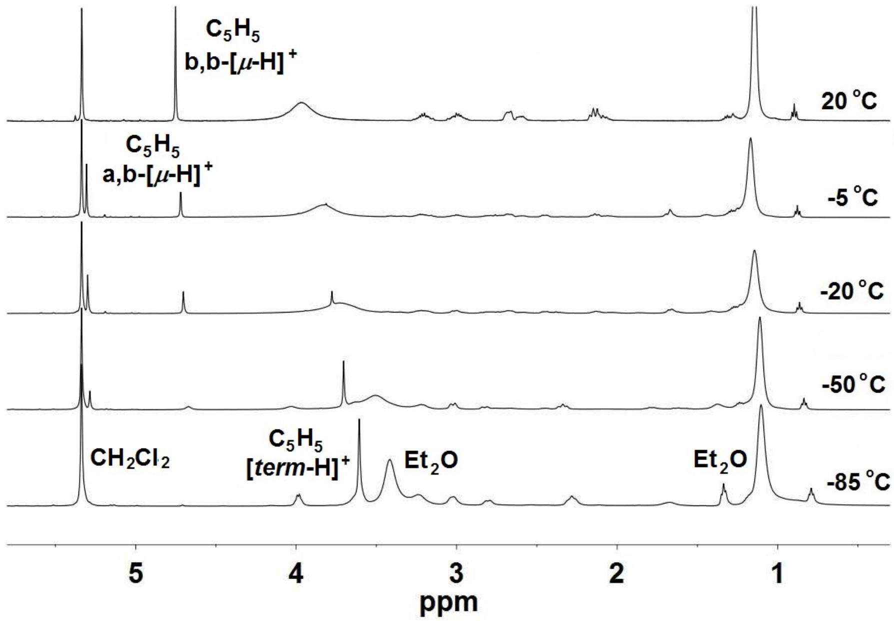

Figure S51. Low field portion of ^{1}H NMR spectra for the low-temperature (−85 ºC) protonation of CpCo(pdt)Fe(CO)(dppe) (**4d**) with one equiv [H(OEt$_2$)$_2$]BAr$^F{}_4$ in CD$_2$Cl$_2$ followed by warming to the indicated temperatures. For the high field portion of the same spectra, see Figure 9 in the paper.

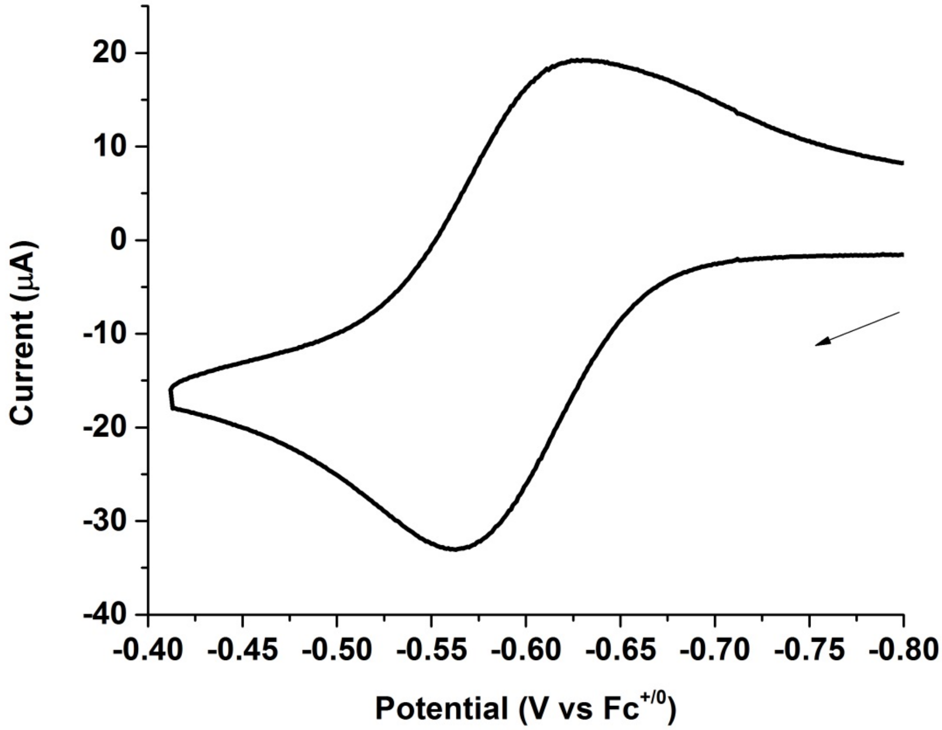

Figure S52. Cyclic voltammogram of CpCo(pdt)Fe(CO)$_2$(dppe) (**4d**) in CH_2Cl_2. *Conditions:* See Figure S42.

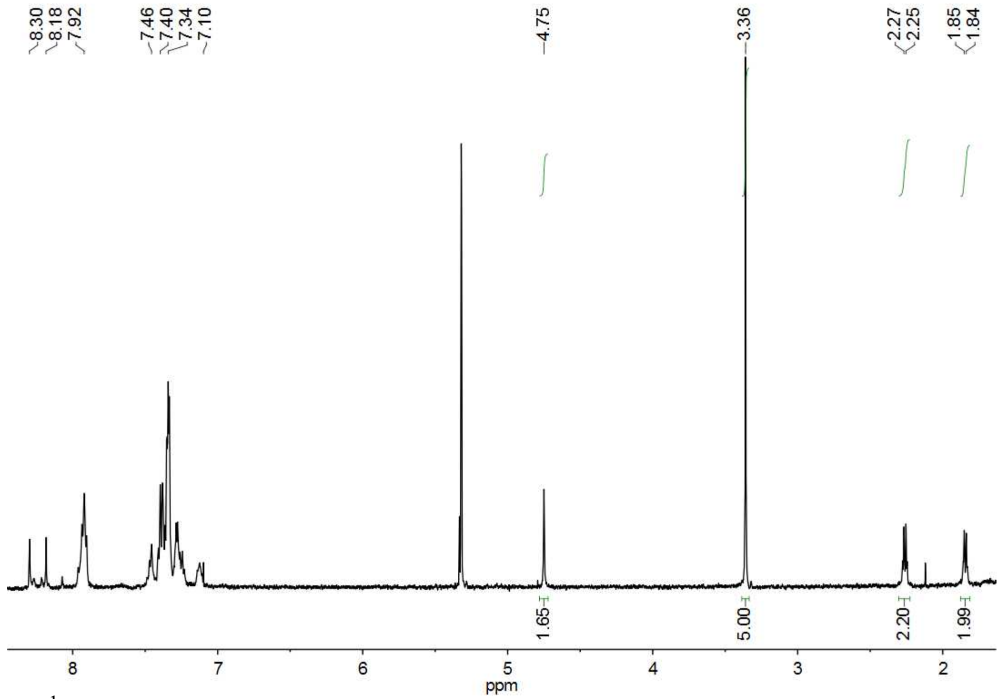

Figure S53. ^{1}H NMR spectrum of CpCo(edt)Fe(CO)(dppv) (**4a**) in CD_2Cl_2.

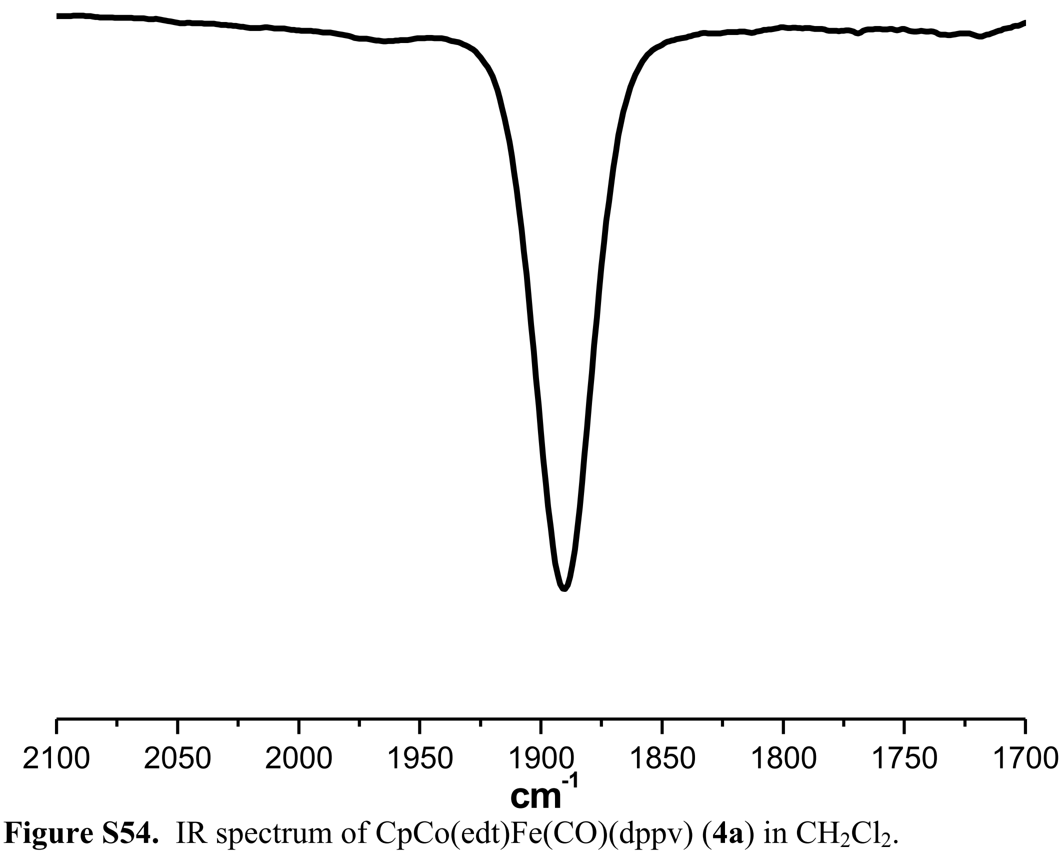

Figure S54. IR spectrum of CpCo(edt)Fe(CO)(dppv) (**4a**) in CH_2Cl_2.